*J. Fluid Mech.* (1995), *vol.* 304, *pp.* 231–262



# A new boundary layer resonance enhanced by wave modulation: theory and experiment

By J. J. HEALEY

University of Cambridge, Department of Engineering, Trumpington Street, Cambridge CB2 1PZ, UK

(Received 3 April 1995 and in revised form 17 August 1995)

When more than one wave is present in a system there exists the possibilty of a resonant interaction. Resonant modes become nonlinear at smaller amplitudes than nonresonant modes. If the nonlinearity causes increased growth rates then it may be that, for a time at least, the behaviour of the resonant modes will be the dominant feature. In shear layers resonant triads can be found where two oblique modes resonate with a plane wave and this case has received much attention in the literature. For a given plane wave, the resonance condition selects oblique modes of a certain wave angle and agreement has been found between predicted wave angles and those measured in experiments.

In this paper it is shown that resonance conditions can also be met between two planar waves in a Blasius boundary layer, where one of the waves is the usual unstable mode, and the other is a higher-order damped mode. The effects of wave modulation are modelled by performing a spatial analysis but allowing the frequency to become complex. It is found that for certain complex frequencies the strength of the nonlinear resonant interaction coefficients is greatly increased. Experiments have been performed in a low-turbulence wind tunnel in which disturbances with modulated and unmodulated sections were introduced into the boundary layer over a flat plate. It was found that disturbances with the frequency and modulation predicted by the theory do indeed show a much greater susceptibility to nonlinear breakdown than nonresonant disturbances.

## 1. Introduction

This paper is concerned with the growth of small-amplitude disturbances in an otherwise laminar zero-pressure-gradient boundary layer. Such disturbances can initiate transition to a turbulent state, and so their study is of considerable practical importance as well as being of intrinsic interest.

When a two-dimensional exciter, e.g. a vibrating ribbon, is used to introduce disturbances into a boundary layer, two-dimensional viscous instability waves (Tollmien–Schlichting modes) are found to propagate and grow downstream for a certain range of excitation frequencies. Flow visualization experiments show that these initially planar waves become three-dimensional before undergoing a transition to turbulence. A possible mechanism causing the oblique waves to grow is the Craik resonant triad in which a plane wave with streamwise wavenumber $\alpha$ and frequency $\omega$ interacts with a pair of oblique modes with $(\alpha/2, \pm\beta, \omega/2)$, where the spanwise wavenumber $\beta$ is chosen so that all three waves have the same phase velocity in the streamwise

direction, see Craik (1971). When the amplitude equations for these waves are calculated, Craik found that the first nonlinear terms are quadratic rather than the usual cubics found for nonresonant modes. This means that the resonant modes become nonlinear 'sooner' than nonresonant modes. Resonant triads are not just important in boundary layers but have been found in many different wave systems, see Craik (1985).

Raetz (1959) was the first to suggest that 2:1 resonances (where, like that studied by Craik, at least two waves are found with the same phase speed and the frequency and streamwise wavenumber of one are twice those of the other) could occur in the Blasius boundary layer for three-dimensional waves. Kelly (1968) showed how resonant interaction can serve to increase the transfer of energy from the mean flow to the disturbance for an inviscid shear layer. Like Kelly's resonance, the resonance described in the present paper is for a pair of two-dimensional spatial waves but is for viscous disturbances in the Blasius boundary layer. The amplitude equations for this 'resonant dyad' have the same form as those in Kelly and are a special case of the resonant triad equations.

More recently, workers developing rational asymptotic theories for nonlinear disturbances have derived amplitude equations that do not have the simple polynomial structure found above. Instead, the nonlinear terms involve integrals which account for upstream history effects and so are nonlocal. These terms, which arise because the nonlinear evolution of the disturbance is determined by nonlinear critical layer effects, were first calculated by Hickernell (1984).

Mankbadi, Wu & Lee (1993) have calculated resonant-triad amplitude equations for the Blasius boundary layer that take account of the nonlinear critical layer effects and have integral terms. This analysis is based on the upper-branch asymptotic scaling of the neutral curve where the critical layer is separate from the viscous wall layer. Near the neutral curve, on this scaling, the growth rates are very small and so this weakly nonlinear analysis might be expected to be valid over a wide range of parameters. However, calculations presented in Healey (1995*a*) indicate that this upper-branch structure is destroyed abruptly at a well defined, and extremely high, Reynolds number $R$. Below this $R$ the disturbance structure reverts to that of the triple-deck theory with the critical layer lying within the viscous wall layer. Further calculations presented in Healey (1995*b*, *c*) show that the weak growth rates associated with the asymptotic upper-branch are also lost, and that for lower $R$ the growth rates near the upper branch are of comparable strength to those of the lower branch. Thus, it seems that the assumption of an asymptotic upper branch disturbance structure used by Mankbadi *et al.* is not justified at transitional Reynolds numbers.

It should be noted, however, that Healey (1995*a*) also found that the value of $R$ above which the asymptotic upper-branch structure exists is very sensitive to the pressure gradient, and that small adverse pressure gradients can greatly reduce this value. Thus, it may be that the resonant-triad amplitude equations for a boundary layer in an adverse pressure gradient derived by Goldstein & Lee (1992), who inspired the work of Mankbadi *et al.*, could well be appropriate at experimentally realizable Reynolds numbers.

An alternative rational asymptotic theory for resonant-triad interactions has been developed by Smith & Stewart (1987), where weak growth rates are found in the downstream limit of the triple-deck theory described in Smith & Burggraff (1986). Although the amplitude equations have the same quadratic form as Craik (1971), it turns out that the nonlinear coefficients are purely imaginary and equisigned.

This leads to conservative coupling and precludes the possibility of the finite time singularity that Craik found. However, this triple-deck limit can also be identified in the high-$R$ Orr–Sommerfeld (OS) calculations presented in Healey (1995*c*) and it happens that this part of the dispersion relationship is only found when $R$ is unrealistically large.

It seems that for the Blasius boundary layer rational asymptotic weakly nonlinear theories can only be developed at values of $R$ very substantially greater than those accessible to experiment. Hultgren (1987) has developed a composite asymptotic theory that captures both upper and lower branches of the neutral curve. This dispersion relation shows the same kink in the neutral curve found by Healey (and also by Reid 1965) that marks the change in structure on the upper branch and gives good quantitative agreement with the OS theory at high enough $R$. However, the extension to a weakly nonlinear theory still requires formally small growth rates and these are only found (for both the composite theory and the OS theory) at extremely high $R$. For this reason, in the present paper a less rigorous approach will be taken where finite, but numerically small, growth (and decay) rates will be used as small parameters in a weakly nonlinear analysis. While not 'rational' it is hoped that some insight into the nonlinear dynamics at transitional $R$ might be obtained.

In §2 evidence is presented for a new resonance where a pair of two-dimensional waves is found such that the fequency and wavenumber of one are exactly twice the other. This resonance was identified using OS theory, but can also be studied using triple-deck theory. This is not a parametric resonance like the resonant triad since in this case it is the fundamental mode which is unstable and the harmonic which is damped according to linear theory. A set of quadratic amplitude equations is derived for this resonant dyad in §3. Although the growth rates of the two modes are finite they will be treated as small parameters in a multiple-scales calculation (they are small in the same sense that $\pi^{-1}$ is small, see page 23 of Lin 1955!). For the case of finite growth rates there is no formal justification for truncating the amplitude equations at quadratic order. However, in §4 it is shown that the quadratic interaction coefficients have an unexpected behaviour if the frequency used in the spatial analysis is allowed to become complex. Physically, the complex frequency is interpreted as a simple model for a modulated wavetrain. For certain complex frequencies the strength of the quadratic interaction increases very dramatically. It may be that this feature is sufficiently robust that it can cause a strong physical effect even if higher-order terms are included. In §5 a bifurcation analysis of these equations is presented showing the complexity of the solutions (including homoclinic orbits, period-doubling bifurcations and chaos).

In order to test whether this resonance, and in particular the effects of modulation, have any relevance in boundary layer transition, a set of experiments have been carried out in the low-turbulence wind tunnel in the Engineering Department at Cambridge University. Controlled disturbances were introduced into the boundary layer at some upstream location and their evolution measured using hot-wire anemometry. These experiments are described in §6. A range of frequencies and modulations were tested, but the strongest nonlinear breakdown was found to occur for the case of a frequency at the resonant frequency predicted by the theory and for the modulation that the theory predicted would be most dangerous. Three-dimensional waves will be present in the experiment (the disturbances were introduced via a point source) and have not yet been included in the theory. Nonetheless, the proposed selection mechanism for a particular resonant two-dimensional frequency does receive strong support from the experimental observations. Conclusions are presented in §7.

## 2. Resonance with a higher-order damped mode

The possibility of a 2:1 resonance is of interest since it can cause the disturbance to become nonlinear at smaller amplitudes than nonresonant modes. While resonant triads have been found in many wave systems, they are not the only way in which this kind of resonance can occur. In addition to Kelly's resonance, Proctor & Jones (1988) have proposed a thermal convection problem in which two two-dimensional modes can be found that satisfy a 2:1 resonance. Ffowcs Williams & Guo (1991) have considered a 2:1 resonance that can occur between the surface modes of a bubble and volume pulsation modes. In both cases quadratic amplitude equations were obtained with the same form as those of Kelly (1968) and Craik (1971).

It is thought that such a resonance cannot occur among purely two-dimensional waves in a flat-plate boundary layer; hence the concentration of interest in the resonant triad. However, in Healey (1994) an investigation was carried out into the OS dispersion relationship where both frequency and wavenumber were allowed to become complex. The extra parameter introduced into the problem (the imaginary part of the frequency) allowed a pair of eigenvalues $(\omega, \alpha)$ to be found such that $(2\omega, 2\alpha)$ are also eigenvalues. However, in order to derive amplitude equations, it is only necessary that the real parts of the eigenvalues should satisfy the resonance condition; the imaginary parts determine the linear growth rates and these should be small compared with the real parts. It turns out that although the resonance found in this paper exactly satisfies the necessary relationship for the real parts of the eigenvalues, the imaginary parts are finite. For this reason, the resonance should perhaps be described as approximate.

Physical quantities will be nondimensionalized using the length, time, velocity and pressure scales $\delta$, $\delta/U_0$, $U_0$ and $\rho U_0^2$ respectively where $\delta$ is the displacement thickness given by

$$\delta = 1.7208\left(\frac{xv}{U_0}\right)^{1/2}, \tag{2.1}$$

$U_0$ is the free-stream velocity, $x$ is the streamwise coordinate, $\rho$ is the density and $v$ is the kinematic viscosity. The presence of $x$ in (2.1) means that a physical wave with fixed frequency will have a nondimensional frequency that increases with downstream distance due to the increasing boundary layer thickness. Nonetheless, this choice is natural when using the OS theory since in the parallel flow approximation any such streamwise variation is neglected; this choice gives a close analogy with plane Poiseuille flow where OS theory is exact. The Reynolds number is then given by

$$R = \frac{\delta U_0}{v}. \tag{2.2}$$

Linearized disturbances, $v(y)e^{i(\alpha x-\omega t)}$, are assumed to satisfy the OS equation,

$$(\alpha U-\omega)(v''-\alpha^2 v)-\alpha U''v+\frac{\mathrm{i}}{R}(v''''-2\alpha^2 v''+\alpha^4 v)=0, \tag{2.3}$$

where $U(y)$ is the mean flow (in this case the Blasius profile), primes denote differentiation with respect to $y$ and $v$ is the vertical component of the two-dimensional velocity perturbation that has frequency $\omega$ and wavenumber $\alpha$. Equation (2.3) is solved subject to the homogeneous boundary conditions $v = v' = 0$ at $y = 0$ and as $y \to \infty$ giving an eigenvalue problem. In a spatial calculation a real $\omega$ and $R$ are given and $\alpha$, which may be complex, must be determined. The spatial problem is the relevant one for boundary layers since in practice, a well-defined frequency of

disturbance is often imposed on the boundary layer which is then observed to either grow or decay downstream. The real part of $\alpha$ then gives the wavelength of the disturbance and the imaginary part gives the growth rate. In what follows, the real and imaginary parts of a complex quantity will be denoted by the subscripts $r$ and $i$ respectively. If $\alpha_i < 0$ then the disturbance grows downstream.

There is no reason why (2.3) should not be solved when $\omega$ is also complex. In fact, this analytic continuation into the complex plane is essential in solving initial value problems, and is a useful computational method for locating branch points and finding higher-order modes. A disclaimer is often given that complex frequencies are not physical, but in §4 it will be argued that a case can be made for giving a physical interpretation to complex frequencies in a localized sense.

Equation (2.3) has been solved using a compound matrix method based on Davey (1982), the actual source code being kindly provided by Professor M. Gaster. Although OS theory is exact only when the base flow is parallel, and the Blasius boundary layer is nonparallel, its use can be given the following justification. The asymptotic theories of Smith (1979) and Bodonyi & Smith (1981) show how nonparallel effects can be systematically included in the linear stability theory and how they affect the position of the lower and upper branches respectively. Nonparallelism enters the expansions for both branches at a relatively high order showing that the Blasius flow is well approximated by the parallel flow assumption. The discrepancy between the upper-branch asymptotics and the OS neutral curve at transitional $R$ is not an indication of nonparallelism (as suggested in Bodonyi & Smith) but, as shown by Healey (1995*a*), can be related to a branch point in the dispersion relation lying at high $R$ near the upper branch. Recent, and very careful, experiments by Klingmann *et al.* (1993) confirm that the OS neutral curve compares well with experiment even at the lowest $R$; see also the numerical calculations by Bertolotti, Herbert & Spalart (1992).

The solid curve in figure 1 represents a continuation of the neutral curve into the complex frequency plane at a fixed Reynolds number. The two intersections of this curve with the dotted line $\omega_i = 0$ give the lower and upper branches of the neutral stability curve. At large enough positive $\omega_i$, all the modes are spatially damped: this is key to the initial value problem. Likewise, at large enough negative $\omega_i$, all the waves are spatially growing; however, it would be dangerous to describe these modes as being more unstable than the $\omega_i = 0$ modes since they are simultaneously suffering a strong temporal decay. The circles correspond to the resonance found in Healey (1994). The dashed lines show that, by relaxing the 2 : 1 condition on the imaginary parts, it is possible to follow the resonance onto the real frequency axis. At first sight this appears to contradict the assertion made earlier that resonance cannot be found for two-dimensional waves. In fact the harmonic mode has passed, relative to the fundamental, around the branch point marked by the cross in figure 1. Thus for real frequencies the resonance is between the unstable mode and one of the higher-order damped modes, i.e. a disconnected branch.

Figure 2 shows the dispersion relationships for these two modes and the resonant frequencies. Straight lines passing through the origin correspond to constant phase speeds. It is clear from the figure that if only the unstable mode is considered then any such line will pass through $\alpha_r^{(1)}$ at most only once (unless the frequency is very small but then the waves would all be damped). Thus with only the unstable mode present no resonance can be found unless oblique modes are also considered. When the second mode is included, there is a range of frequencies for which pairs of waves can be found that both travel at the same phase speed, i.e. straight lines that pass

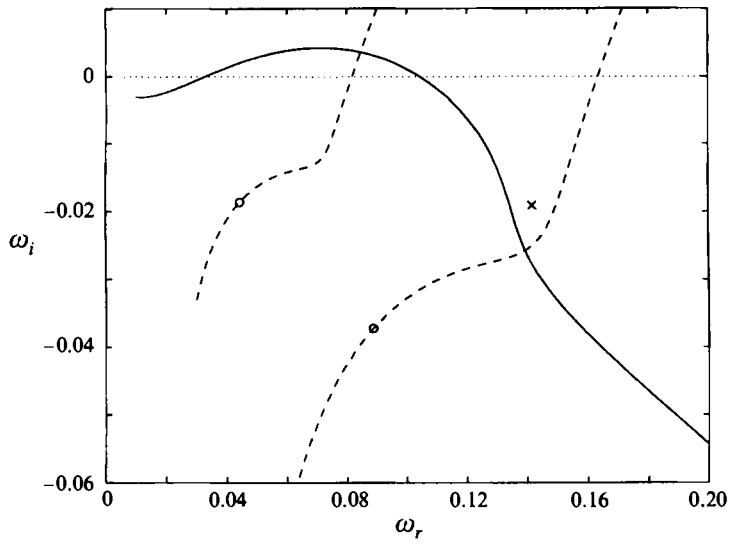


FIGURE 1. Extension of a spatial analysis for complex frequencies at $R = 2000$. The solid line is where $\alpha_i = 0$, below this line $\alpha_i < 0$ and the modes grow in the downstream direction. The circles correspond to a pair of eigenvalues $(\omega, \alpha)$ for which $(2\omega, 2\alpha)$ are also eigenvalues. The dashed lines show the locus of points which satisfy the real part resonance such that $(\omega, \alpha_r)$ and $(2\omega, 2\alpha_r)$ are all eigenvalues. The cross marks a branch point where two modes meet.

through the origin and intersect both $\alpha_r^{(1)}$ and $\alpha_r^{(2)}$. However, there is only one such pair where one wave has exactly twice the frequency as the other, and this pair is marked by '+' symbols in the figure. At $R = 2000$ the resonance occurs at $\omega = 0.0817$ and the wavenumbers are $\alpha^{(1)} = 0.256 - 0.0101\mathrm{i}$ and $\omega = 0.1634$, $\alpha^{(2)} = 0.512 + 0.225\mathrm{i}$. Incidently, the reason that the damped mode ends abruptly is that as $\omega$ decreases, its phase velocity increases and approaches unity near $\omega = 0.034$, hence this mode is approaching the continuous spectrum.

This behaviour is not particular to this Reynolds number. Figure 3 shows how well much of the complex frequency data collapse when the lower-branch Reynolds number scaling is used. As expected, there is good collapse of the neutral curves near the lower branch (i.e. the low-frequency intersection of the neutral curves with the real frequency axis) for all the Reynolds numbers considered. There is even a reasonable data collapse for the upper branch (i.e. the high-frequency intersection of the neutral curves with the real frequency axis) for $2000 \leqslant R \leqslant 10000$, but between $R = 5 \times 10^4$ and $R = 2 \times 10^5$ there is a relatively large movement in the position of the upper branch. This corresponds to the kink in the neutral curve found near $R = 10^5$ in Healey (1995*a*). For $R > 10^5$ the upper-branch neutral curves clearly do not scale as $R^{-1/2}$. The neutral curve passes through the branch point for a Reynolds number between 6000 and 7000 and the discontinuous movement in the neutral curve at large negative $\omega_i$ between these values of $R$ is a consequence of branch-switching. At $R = 7000$ the neutral curve bends sharply as it passes over the top of the branch point, and it is the remnants of this sharp bend that causes the kink in the neutral curve at higher $R$ for real frequencies.

The dashed curves show the resonant modes, and all of these collapse well over the range $2000 \leqslant R \leqslant 10^6$ suggesting that they have a triple-deck structure. In fact, analysis of the leading-order triple-deck dispersion relationship, e.g. setting $\epsilon = 0$ in equation (4) of Hultgren (1987), shows that the resonance occurs at $\omega = 2.85R^{-1/2}$,

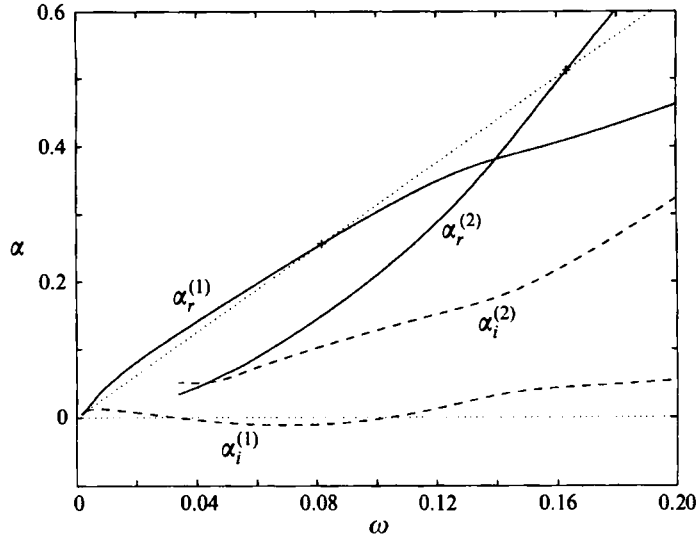


FIGURE 2. Dispersion relationships for the modes that can resonate at $R = 2000$ for real frequencies. The solid lines are the real parts of the wavenumbers and the dashed lines are the imaginary parts. The superscript (1) corresponds to the usual unstable mode and (2) corresponds to the higher-order damped mode. The 'plus' symbols show the resonant modes.

$\alpha^{(1)} = (1.14 - 0.149\mathrm{i})R^{-1/4}$ and $\alpha^{(2)} = (2.28 + 0.865\mathrm{i})R^{-1/4}$ as $R \to \infty$. The branch point that separates the resonant modes is the same branch point that causes the kink in the neutral curve. Incidently, Hultgren mentions in his paper that there is a 'distinct possiblity' that parametric resonance may exist for a higher-order mode.

## 3. Nonlinear amplitude equations

The resonance identified in the previous section is between the unstable mode and a higher-order damped mode. Both modes are found on the triple-deck dispersion relation and have $O(1)$ growth rates compared with the real parts of the wavenumbers. At $R = 2000$ the growth and decay rates, $|\alpha_i|/\alpha_r$, of the two modes are 0.039 and 0.44, and as $R \to \infty$ these rates become 0.13 and 0.38. In this section, it will be assumed these growth rates can be considered to be small compared with one. The resulting truncated amplitude equations are not rigorously justified, but there are examples in boundary layer stability when asymptotic theories give reasonable results even when the small parameter is not so small. A simple example is the leading-order triple-deck estimate for the resonant frequency given at the end of §2. This result was obtained by assuming that terms $O(\epsilon)$ could be ignored in Hultgren's expression, where $\epsilon = (\omega/R)^{1/6}$. When $R = 2000$, $\epsilon = 0.19$ at resonance, and the difference between this resonant frequency and the OS resonance is 20%. If the $O(\epsilon)$, $O(\epsilon^2)$ and $O(\epsilon^3 \ln \epsilon)$ terms are included, then the triple-deck resonant frequency is only 2.6% away from the OS value despite the fact that the neglected terms are only $|\ln \epsilon| = 1.6$ times smaller than the retained terms.

A further possible justification for using weakly nonlinear theory for this case is that the ratio $\gamma$ of the unstable growth rate to the damping rate of the higher-order mode is relatively small. At $R = 2000$, $\gamma = 0.045$, and near $R = 810$, $\gamma = 0$. Hughes & Proctor (1990; 1992) have studied resonant interactions in the limit $\gamma \to 0$. They found that the dynamics become independent of $\gamma$. In other words, it does not matter how

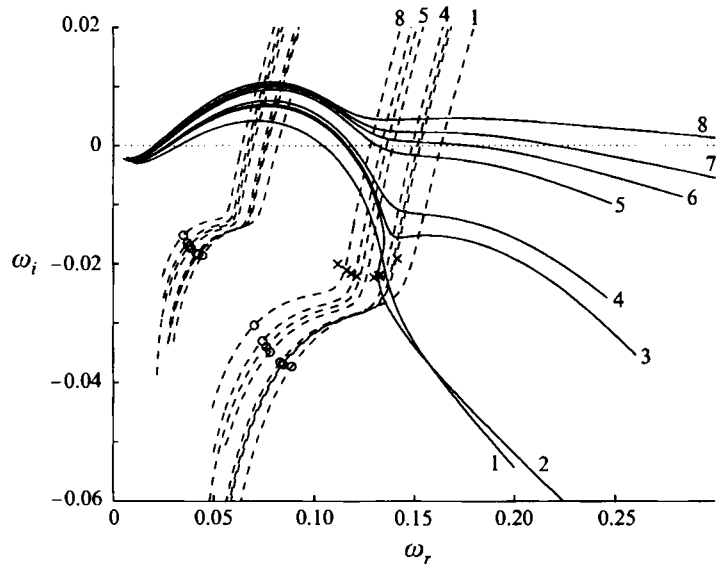


FIGURE 3. Same as figure 1 but with the results for eight different Reynolds number superimposed and scaled by $R^{-1/2}$. The lines marked by $1, 2, \ldots, 8$ have $R = 2 \times 10^3$, $6 \times 10^3$, $7 \times 10^3$, $10^4$, $5 \times 10^4$, $10^5$, $2 \times 10^5$ and $10^6$ respectively. All of the dashed lines for the harmonics pass to the right of their respective branch points. The neutral curves 1 and 2 pass under the branch point, the rest pass over it.

strongly damped the damped mode is (though it must still be small compared with one) or how weakly amplified the unstable mode is provided that one is much smaller than the other. This situation is somewhat analogous to that of the centre-manifold in dynamical systems theory: the dynamics on the centre-manifold are independent of how strong the contraction onto the centre-manifold is. In the present case it is the damped mode that most compromises the assumption of weakly nonlinear behaviour and so terms involving this mode will be least accurate. However, since $\gamma$ is small, this might not be a serious shortcoming. Of course, ultimately the use of weakly nonlinear theory can only be justified if it turns out to have some relevance to experiments on boundary layer transition.

The amplitude equations have been derived using a multiple scales approach like that in Proctor & Jones (1988). A small spatial detuning from the exact resonance will be included in the analysis. The small parameter in the expansion, $\epsilon$, is given by the growth rate of the unstable mode. The resonant wavenumbers for a real frequency $\omega$ are then written as

$$\alpha^{(1)} = \alpha_r - \mathrm{i}\epsilon, \tag{3.1}$$

$$\alpha^{(2)} = 2\alpha_r + \Delta\epsilon + \mathrm{i}\epsilon/\gamma, \tag{3.2}$$

where $\Delta$ is the detuning parameter ($\Delta = 0$ implies exact resonance) and $\gamma$ is the ratio of the growth rates. As noted above, $\epsilon = \gamma = 0$ at $R \approx 810$, $\epsilon/\alpha_r \to 0.131$ and $\gamma \to 0.172$ as $R \to \infty$, and $\epsilon/(2\alpha_r\gamma) \approx 0.4$ for all $R$. The oscillations occur on the fast scale $x$ and the amplitude of the waves varies on a slow scale $X = \epsilon x$. Hence the resonant modes have the form

$$A_1(X)E + \text{c.c.} \quad \text{and} \quad A_2(X)E^2 + \text{c.c.} \tag{3.3}$$

where

$$E = \mathrm{e}^{\mathrm{i}(\alpha_r x - \omega t)}, \tag{3.4}$$

and c.c. denotes the complex conjugate of the preceding terms. The velocities and pressures are expanded as a power series in $\epsilon$:

$$u = U + \epsilon(A_1 u_1 E + A_2 u_2 E^2) + \epsilon^2(u_{21} E + u_{22} E^2) + \text{c.c.}, \tag{3.5}$$

$$v = \epsilon(A_1 v_1 E + A_2 v_2 E^2) + \epsilon^2(v_{21} E + v_{22} E^2) + \text{c.c.}, \tag{3.6}$$

$$p = \epsilon(A_1 p_1 E + A_2 p_2 E^2) + \epsilon^2(p_{21} E + p_{22} E^2) + \text{c.c.}, \tag{3.7}$$

where $U = U(y)$ is the Blasius profile and the subscripted $u$, $v$ and $p$ terms are functions of $y$ only. The first- and second-order spatial derivatives are written in the usual way as

$$\frac{\partial}{\partial x} + \epsilon \frac{\partial}{\partial X} \quad \text{and} \quad \frac{\partial^2}{\partial x^2} + 2\epsilon \frac{\partial^2}{\partial x \partial X} \tag{3.8}$$

respectively and (3.5)–(3.8) are substituted into the Navier–Stokes equations for two-dimensional incompressible flow. The resonance generates inhomogeneous terms at $O(\epsilon^2)$ and application of the appropriate solvability conditions leads to the following amplitude equations:

$$\dot{A}_1 = A_1 + a A_1^* A_2, \tag{3.9}$$

$$\dot{A}_2 = -(\gamma^{-1} - \mathrm{i}\Delta) A_2 + b A_1^2. \tag{3.10}$$

The details of this derivation and the definitions of the complex nonlinear interaction coefficients $a$ and $b$ are given in Appendix A.

## 4. Wave modulation

It has been observed in experiments, see Gaster (1979), that modulated waves can be more susceptible to a nonlinear beakdown than unmodulated wavetrains. Gaster reported that a wave packet can show nonlinear behaviour at an amplitude 'some four or five times smaller' than a pure monochromatic wavetrain. More recent experiments by Shaikh & Gaster (1994) have been performed in which randomly modulated wavetrains were introduced into the boundary layer. Again it was found that modulation plays an important role in the enhancement of nonlinear behaviour. Although the input disturbance had a flat spectral content, like an impulse, the nonlinear breakdown was highly localized and completely reproducible. This suggests that particular sorts of modulation are somehow more dangerous than others.

Stewartson & Stuart (1971) have developed a weakly nonlinear theory for wave packets in plane Poiseuille flow and Hocking (1975) has extended this analysis to the case of the asymptotic suction profile. In both cases the amplitude is taken to be a slowly varying function of both $x$ and $t$ (and also $z$) rather than just $x$ as in the previous section. The amplitude then satisfies a partial differential equation. In this section a simpler approach will be adopted that leaves the structure of (3.9) and (3.10) intact.

In the conventional spatial analysis the frequency is taken to be real and this models a disturbance whose amplitude is constant in time at a particular position in the boundary layer. If the frequency is taken to be complex with positive imaginary part then this models a disturbance whose amplitude is growing exponentially in time at a particular point in the boundary layer. A disturbance with exponentially increasing amplitude can be introduced to the boundary layer in an experiment, but

only for a finite period of time because eventually the amplitude becomes too large for the linear theory to be appropriate. Although the amplitude of a complex frequency becomes arbitrarily large as $t \to \pm\infty$ (depending on the sign of the imaginary part), the notion of a complex frequency that exists for a finite time (or even a semi-infinite time) that is long compared to the period of the oscillation may be useful. In fact, this method of modelling modulation could be used whenever the operator $\partial/\partial t \equiv -\mathrm{i}\omega$, e.g. in numerical solutions of the linearized spatial Navier–Stokes equations or in solving the parabolized stability equations developed by Herbert, see Bertolotti *et al.* (1992).

The decomposition of a signal into frequencies which are localized in time is precisely what is done when using a wavelet transform. Farge (1992) has recently reviewed the use of the wavelet transform in fluid mechanics. A time series $f(t)$ can be decomposed into a set of wavelet coefficients $W(t_0, s)$ where $s$ is a parameter that characterizes a scale or frequency in the signal and $t_0$ is a point in the time series. The magnitude of a wavelet coefficient gives a measure of the energy in the signal at a particular point in the time series of a particular frequency. A wavelet $g(t;s)$ is chosen which, for a fixed value of $s$, gives a shape that has a simple structure and is localized with a finite amplitude over a period of order $1/s$. A commonly used choice for the wavelet transform is the Morlet wavelet, see equation (23) of Farge (1992), which is given by

$$g(t;s) = \mathrm{e}^{-(st)^2/2 - \mathrm{i}mst}. \tag{4.1}$$

This wavelet is an oscillation with a Gaussian modulation and so resembles a wave packet. The parameter $m$ determines the number of oscillations present in the wavelet; in what follows $m = 5$. For a fixed $s$ the wavelet is translated by $t_0$ and then projected onto the signal, $f(t)$:

$$W(t_0, s) = s^{1/2} \int_{-\infty}^{\infty} f(t) g(t - t_0; s) \mathrm{d}t \tag{4.2}$$

where the factor $s^{1/2}$ is used to normalize the energies in each scale. The expression (4.2) is evaluated most efficiently by taking the Fourier transforms of $f$ and $g$ and performing a convolution in the frequency domain, i.e. let

$$\tilde{f}(\omega) = \int_{-\infty}^{\infty} f(t) \mathrm{e}^{-\mathrm{i}\omega t} \mathrm{d}t, \tag{4.3}$$

$$\tilde{g}(\omega; s) = \int_{-\infty}^{\infty} g(t;s) \mathrm{e}^{-\mathrm{i}\omega t} \mathrm{d}t, \tag{4.4}$$

then let

$$\tilde{h}(\omega; s) = \tilde{f}(\omega) \tilde{g}(\omega; s) \tag{4.5}$$

and hence

$$W(t_0, s) = \frac{s^{1/2}}{2\pi} \int_{-\infty}^{\infty} \tilde{h}(\omega; s) \mathrm{e}^{\mathrm{i}\omega t} \mathrm{d}\omega. \tag{4.6}$$

As an example, consider the function

$$f(t) = \begin{cases} c_1 \sin \omega_r t \mathrm{e}^{\omega_i t} & \text{for } t < t_1 \\ c_2 \sin \omega_r t & \text{for } t_1 < t < t_2 \\ c_3 \sin \omega_r t \mathrm{e}^{-\omega_i t} & \text{for } t > t_2 \end{cases} \tag{4.7}$$

where $\omega_i > 0$ and the constants $c_1$, $c_2$ and $c_3$ are chosen to ensure that $f$ is continuous. This function is shown in figure 4($a$) and can be thought of has being the real part

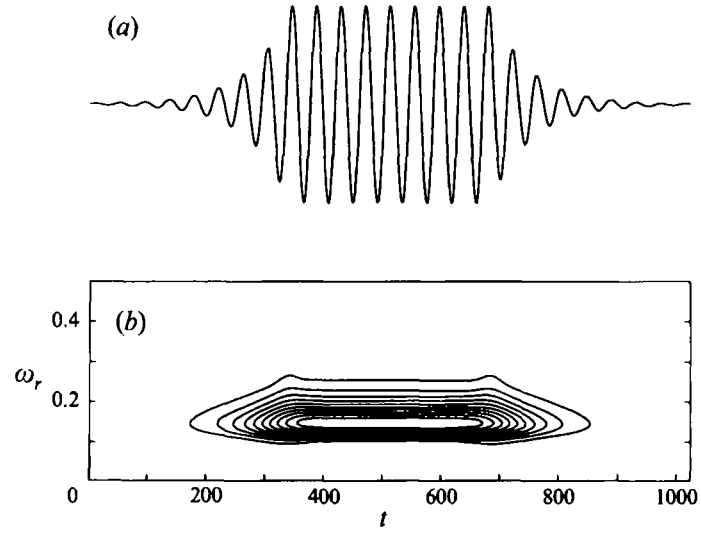


FIGURE 4. (*a*) A plot of $f(t)$ defined by (4.1) using $\omega_r = 0.15$ and $\omega_i = 0.015$. (*b*) A contour plot of the magnitude of the wavelet coefficients calculated using (4.7) and $\omega_r = 5s$ which is the frequency of the oscillation within the wavelet ($m = 5$). Discrete fast Fourier transforms were used and $f(t)$ was sampled at period $\tau = 1$ giving a Nyquist frequency of 0.5.

of a signal consisting of two complex frequencies with oppositely signed imaginary parts with a section of real frequency in the middle. For times such that $\omega_r|t - t_1| \gg 1$ and $\omega_r|t - t_2| \gg 1$, each section of this composite signal will evolve independently as the disturbance propagates downstream. Dispersion will occur for $t \approx t_1$ and $t \approx t_2$. In this sense, parts of a modulated time series can behave locally like complex frequencies. Of course, $f(t)$ can be equally well described by a sum of Fourier modes, and for linear disturbances there can be no advantage in using the idea of complex frequencies, but for the nonlinear analysis it may be simpler, and physically more intuitive, to represent a modulated disturbance by a small number of local complex frequencies.

The wavelet transform of (4.7) is shown in figure 4(*b*). The frequency of the central unmodulated section is picked out very clearly and the amplitude of this frequency is seen to increase and decrease on either side. There is leakage into other frequencies owing to the compact nature of the wavelets, but there is extra leakage near $t_1$ and $t_2$ where there are discontinuities in the first derivative of the envelope function. This wavelet transform plane can also be used to estimate the values of $\omega_i$ corresponding to each frequency at any given instant in time. At a particular value of $s$, and hence $\omega_r$, $\omega_i$ can be estimated from the rate of change of amplitude of that frequency at that moment in time:

$$\omega_i(t, s) = \frac{1}{\tau} \ln \left\{ \frac{|W(t+\tau, s)|}{|W(t, s)|} \right\} \tag{4.8}$$

where $\tau$ is the sample time. Therefore, at any moment in time, it is possible to decompose the signal in a way that shows how the energy is distributed throughout the complex frequency plane. Figure 5 shows the energy in the complex frequency plane at four different times. In (*a*), which corresponds to a growing part of the time series, the energy of the signal is concentrated near $\omega \approx 0.15 + 0.015\mathrm{i}$. In (*b*) the signal is stronger than in (*a*) and is concentrated on the real axis at $\omega \approx 0.15$. Part (*c*)

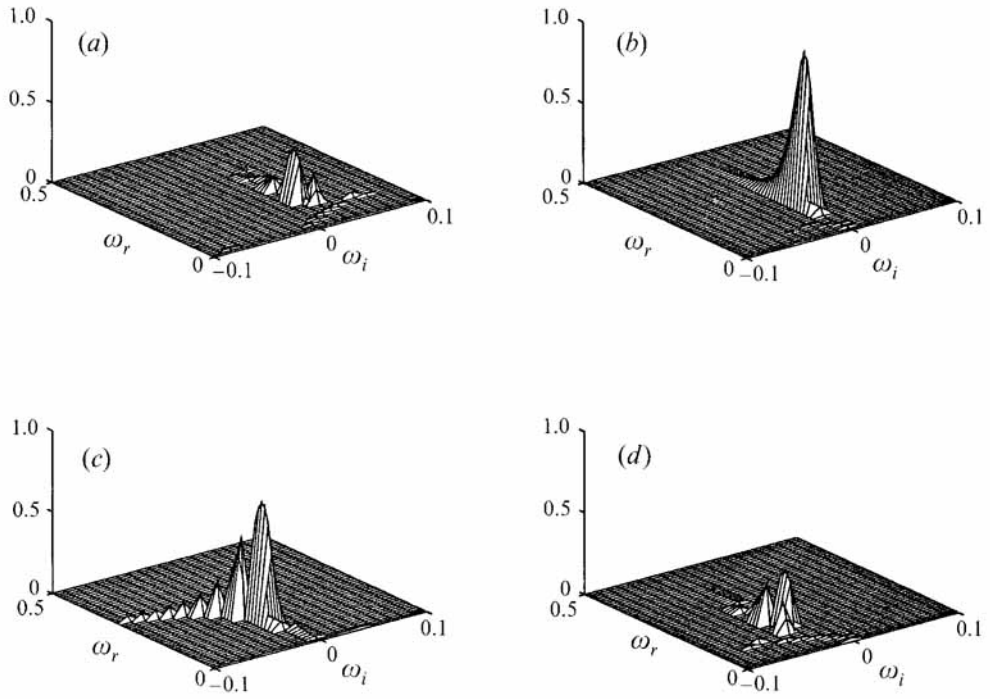


FIGURE 5. Energy distribution over the complex frequency plane at times $t = 260$, 500, 700 and 764, (*a*), (*b*), (*c*) and (*d*) respectively. In each plot the vertical axis is $|W|$.

corresponds to close to the point where $f(t)$ switches from having constant amplitude to a decaying amplitude, and here more frequencies are excited and are spread across the $\omega_i < 0$ half-plane. Part (*d*) is taken from the decaying section of the time series and here the energy is concentrated near $\omega \approx 0.15 - 0.015\mathrm{i}$.

The amplitude equations derived in §3 for real frequencies can be derived in exactly the same way for complex frequencies. The difference is that now, instead of (3.3) and (3.4), the resonant modes are

$$A_1(X)E\mathrm{e}^{\omega_i t} + \text{c.c.} \quad \text{and} \quad A_2(X)E^2\mathrm{e}^{2\omega_i t} + \text{c.c} \tag{4.9}$$

where

$$E = \mathrm{e}^{\mathrm{i}(\alpha_r x - \omega_r t)}, \tag{4.10}$$

as before. The resulting amplitude equations are now

$$\dot{A}_1 = A_1 + a\mathrm{e}^{2\omega_i t}A_1^* A_2, \tag{4.11}$$

$$\dot{A}_2 = -(\gamma^{-1} - \mathrm{i}\Delta)A_2 + bA_1^2. \tag{4.12}$$

Equations (4.11) and (4.12) are to be solved at a constant time $t$ (since this is a spatial calculation). The additional term in $t$ is a consequence of the fact that the strength of the nonlinear interaction must now be a function of time since the amplitudes are now functions of time. Equations (4.11) and (4.12) can be transformed to (3.9) and (3.10) through the rescaling $A_1 \mapsto \mathrm{e}^{-\omega_i t}A_1$ and $A_2 \mapsto \mathrm{e}^{-2\omega_i t}A_2$.

It might seem that allowing complex $\omega$ can only have a small effect on the nonlinear coefficients. However, this need not be the case. Figure 1 shows that for $\omega_i < 0$ the dashed line corresponding to the higher-frequency resonant mode passes close to the branch point. Near the branch point the eigenfunctions undergo rapid changes in

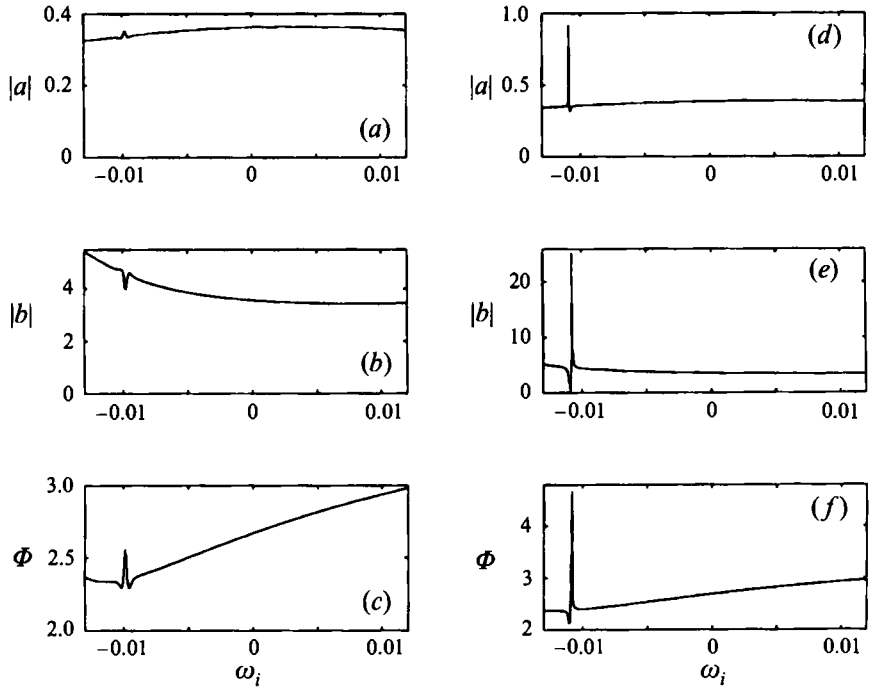


FIGURE 6. Variation of the nonlinear coefficients with the imaginary part of the resonant complex frequency. (*a–c*), are for $R = 1550$, (*d–f*) are for $R = 1350$.

structure, and, since $a$ and $b$ depend on the eigenfunctions via (A 15) and (A 16), these coefficients can also change rapidly. Before continuing, it should be noted that if $\Phi = \arg(-ab)$ then the case $\Phi = 0$ corresponds to conservative coupling, i.e. the modes can exchange energy between themselves but the nonlinear terms do not effect the transfer of energy from the mean flow (see §5 for a fuller discussion). It will be seen below that in general $\Phi \neq 0$.

Figure 6 shows how $|a|$, $|b|$ and $\Phi$ vary with $\omega_i$ at two different Reynolds numbers. At $R = 1550$ the coefficients vary smoothly except near $\omega_i \approx -0.01$ where all three graphs show a relatively small 'blip'. At this Reynolds number the effect of modulation is not likely to have any significant effect on the behaviour of disturbances in a boundary layer. However, at $R = 1350$ all three graphs show a strong spike near $\omega_i \approx -0.011$, in particular $|b|$ increases by a factor of 5 within this narrow region. The spikes occur when the resonant modes are close to the branch point and no such behaviour has been found for $\omega_i > 0$. In both cases $\Phi \neq 0$ and so the increase in the magnitude of the nonlinear coefficient can correspond to increasing the nonlinear transfer of energy from the mean flow to the disturbance.

There is clearly a sensitive dependence of the spikes on Reynolds number, and figure 7 shows how the magnitude of $|b|$ varies across the $(R, \omega_i)$-plane: $|b|$ varies smoothly over most of the plane (as would have been anticipated) except along a locus of points, which correspond to eigenvalues near the branch point, where very sharp variations occur. Figure 2 shows that the resonant modes pass close to the branch point at very large $R$ and so this spiky behaviour can be expected to occur at asymptotically large Reynolds numbers too. The spikes in figures 6 and 7 occur when $|\omega_i|/\omega_r \approx 0.1$, so the rate of modulation required is similar to that in figure 4(*a*).

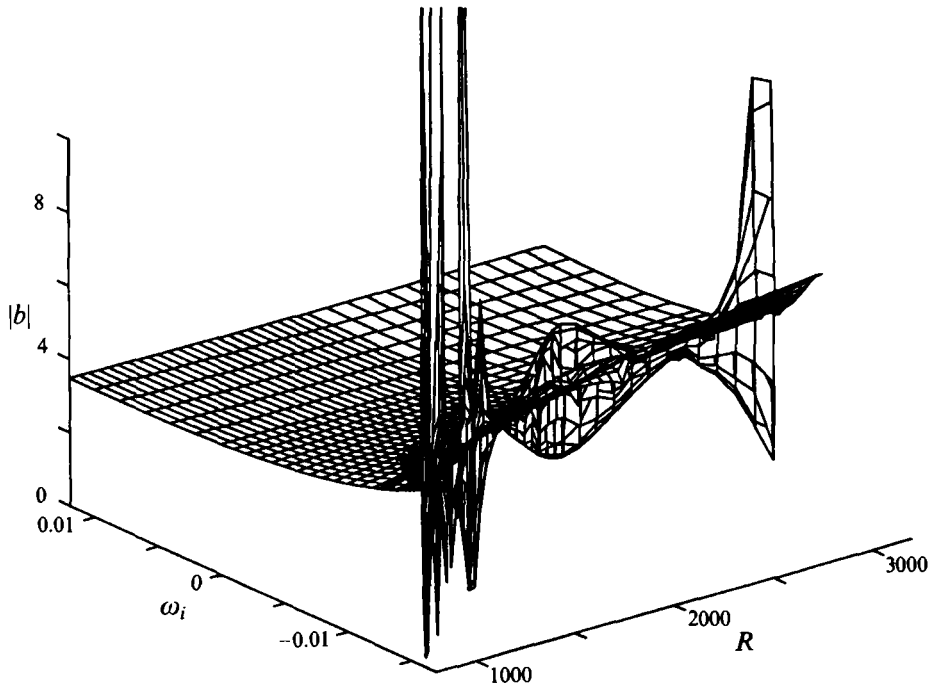


FIGURE 7. Variation of $|b|$ with the imaginary part of the resonant complex frequency and Reynolds number.

If the weakly nonlinear analysis carried out in §3 were extended to higher order then the cubic-, quartic- and higher-order nonlinear terms would have coefficients that have a similar form to (A 15) and (A 16) and would also involve multiples of the eigenfunctions $v_1$ and $v_2$. Thus for resonant modes near the branch point, the higher-order coefficients are likely also to show the same spiky behaviour as the quadratic coefficients. This suggests that even if the truncation at quadratic order is hard to justify, the higher-order nonlinear terms may be showing the same behaviour anyway, and that therefore (3.9) and (3.10) *do* capture important features of the disturbance dynamics in a boundary layer.

## 5. Analysis of the amplitude equations

In order to understand the behaviour of (3.9) and (3.10) it helps to make several changes of coordinates. First, let

$$A_1 = |ab|^{-1/2} B_1, \tag{5.1}$$

$$A_2 = B_2/a, \tag{5.2}$$

then

$$\dot{B}_1 = B_1 + B_1^* B_2, \tag{5.3}$$

$$\dot{B}_2 = -(\gamma^{-1} - \mathrm{i}\Delta) B_2 - \mathrm{e}^{\mathrm{i}\Phi} B_1^2, \tag{5.4}$$

where $\Phi = \arg(-ab)$ as before. The same equations are obtained if (4.11) and (4.12) are used instead; the only difference is that the $a$ in (5.1) and (5.2) is replaced by

$ae^{2\omega_i t}$. The rate of change of energy of the two modes is given by

$$\frac{\partial}{\partial X}\left(|B_1|^2+|B_2|^2\right)/2 = |B_1|^2 - \gamma^{-1}|B_2|^2 + \mathrm{Re}\left\{B_1^2 B_2^*(1-\mathrm{e}^{\mathrm{i}\Phi})\right\} \tag{5.5}$$

where $\mathrm{Re}\{\cdot\}$ denotes the real part. Clearly $\Phi = 0$ means that the nonlinear terms are conservative and for a given $B_1$ and $B_2$ the strongest nonlinear energy transfer occurs when $\Phi = \pm\pi$. Whether the nonlinear terms are stabilizing or destabilizing depends on the sign of the last term in (5.5) and this can be positive or negative depending on the relative phase of $B_1$ and $B_2$. This phase dependence is an important feature of resonant amplitude equations and is not found for nonresonant modes. This property is brought out further by transforming into polar coordinates: let

$$B_1 = r_1 \mathrm{e}^{\mathrm{i}\theta_1}, \tag{5.6}$$

$$B_2 = r_2 \mathrm{e}^{\mathrm{i}\theta_2}, \tag{5.7}$$

where $r_1$ and $r_2$ are real and positive and $\theta_1$ and $\theta_2$ are real, then the amplitude equations may be written

$$\dot{r}_1 = r_1 + r_1 r_2 \cos\chi, \tag{5.8}$$

$$\dot{r}_2 = -\gamma^{-1} r_2 - r_2^2 \cos(\Phi - \chi), \tag{5.9}$$

$$\dot{\chi} = \Delta - \frac{r_1^2}{r_2}\sin(\Phi - \chi) - 2r_2 \sin\chi, \tag{5.10}$$

where $\chi = \theta_2 - 2\theta_1$. Thus the relative phase, $\chi$, between the modes evolves and there is the possibilty that some choices of initial conditions may lead to divergent solutions whereas others, that are identical except for relative phase, may lead to bounded solutions. This property will be tested for in the experiment, see §6.

In order to analyse these equations further, it is convenient to use the following transformation (see Hughes & Proctor 1992) that removes the trigonometric functions of the independent variables and leads to equations in three real variables:

$$x = \gamma r_2 \cos\chi, \tag{5.11}$$

$$y = \gamma r_2 \sin\chi, \tag{5.12}$$

$$z = (\gamma r_1)^2; \tag{5.13}$$

$x$ and $y$ together characterize the amplitude and relative phase of the $r_2$ mode and $z$ characterizes the amplitude of the $r_1$ mode. The amplitude equations finally become

$$\dot{x} = -x - \delta y + 2y^2 - z\cos\Phi, \tag{5.14}$$

$$\dot{y} = \delta x - y - 2xy - z\sin\Phi, \tag{5.15}$$

$$\dot{z} = 2\gamma z + 2xz, \tag{5.16}$$

where the dots denote derivatives with respect to $\gamma X$ and $\delta = \gamma\Delta$. These equations are the same as equations (1.6) of Hughes & Proctor (1992) but with a time reversal and their $\gamma$ is the reciprocal of our $\gamma$. There are three parameters: $\gamma$, $\Phi$ and $\delta$. The first two are functions of $R$ and $\omega_i$ and the third can be chosen arbitrarily (it is the amount of detuning). Equations (5.14)–(5.16) are invariant under the transformation

$$y \mapsto -y, \tag{5.17}$$

$$\Phi \mapsto -\Phi, \tag{5.18}$$

$$\delta \mapsto -\delta, \tag{5.19}$$

so, without loss of generality, we shall restrict ourselves to $\delta < 0$.

The fixed points of (5.14)–(5.16) are found by setting $\dot{x} = \dot{y} = \dot{z} = 0$ and there are nontrivial fixed points located at

$$x = -\gamma, \tag{5.20}$$

$$y = \frac{\delta - (1-2\gamma)\cot\Phi}{4} \pm \frac{1}{4}\left\{(\delta - [1+2\gamma]\cot\Phi)^2 - \frac{8\gamma}{\sin^2\Phi}\right\}^{1/2}, \tag{5.21}$$

$$z = \frac{(2\gamma-1)y - \gamma\delta}{\sin\Phi} \tag{5.22}$$

provided that

$$(\delta - [1+2\gamma]\cot\Phi)^2 \geqslant \frac{8\gamma}{\sin^2\Phi}. \tag{5.23}$$

These fixed points diverge to infinity as $\Phi \to 0$ (there can be no equilibria when $\Phi = 0$), and are created by a saddle-node bifurcation at

$$\delta = (1+2\gamma)\cot\Phi \pm \frac{2(2\gamma)^{1/2}}{\sin\Phi} \tag{5.24}$$

which is obtained by using (5.23) at equality. In addition, it is necessary that $z > 0$ from (5.13). Substituting (5.24) into (5.20) and (5.21) gives

$$z = \frac{2\gamma}{\sin^2\Phi}\left(-\cos\Phi \mp \frac{1+2\gamma}{2(2\gamma)^{1/2}}\right), \tag{5.25}$$

and since

$$\frac{1+2\gamma}{2(2\gamma)^{1/2}} \geqslant 1 \tag{5.26}$$

(with equality when $\gamma = 1/2$) it follows that the saddle-node with $z \geqslant 0$ for all $\Phi$ and $\gamma$ is given by

$$\delta = (1+2\gamma)\cot\Phi - \frac{2(2\gamma)^{1/2}}{\sin\Phi}. \tag{5.27}$$

Physically, a fixed point corresponds to a pair of waves that each has a constant finite amplitude and constant relative phase. The stability of the fixed points is determined by finding the eigenvalues of the Jacobian, $\boldsymbol{J}$, of (5.14)–(5.16) evaluated at the fixed points:

$$\boldsymbol{J} = \begin{pmatrix} -1 & 4y-\delta & -\cos\Phi \\ \delta - 2y & -1-2x & -\sin\Phi \\ 2z & 0 & 2(\gamma+x) \end{pmatrix}. \tag{5.28}$$

The eigenvalues, $\lambda$, of $\boldsymbol{J}$ satisfy the cubic

$$0 = \lambda^3 + l_2\lambda^2 + l_1\lambda + l_0 \tag{5.29}$$

where

$$l_0 = 2(1-2\gamma)(\gamma - 2y^2) - 2\gamma\delta(4y-\delta), \tag{5.30}$$

$$l_1 = 1 + (2y-\delta)(6y-\delta), \tag{5.31}$$

$$l_2 = 2(1-\gamma). \tag{5.32}$$

The fixed points will undergo a Hopf bifurcation if $l_0 = l_1 l_2$ and $l_1 > 0$. The existence of a periodic orbit would correspond to a pair of waves with periodically modulated amplitudes and whose relative phase oscillates about some mean value, and hence they travel with oscillating phase speeds.

In Healey *et al.* (1991) three coupled nonlinear ordinary differential equations were studied that also had steady bifurcations (in that case a pitchfork rather than a saddle-node due to a reflection symmetry) and Hopf bifurcations. It turned out to be particularly fruitful to examine the case when, for certain parameter values, the steady and unsteady bifurcations occur almost simlutaneously. Close to this multiple bifurcation point, called a Takens–Bogdanov point, it is possible to obtain exact solutions by reducing the system to a pair of ordinary differential equations on the centre-manifold, see Guckenheimer & Holmes (1986). Of special interest is a locus of planar homoclinic orbits (an orbit of infinite period that approaches a saddle fixed point as $t \to \pm\infty$) that originate at the Takens–Bogdanov point. It was found that far enough away, where the centre-manifold reduction no longer applies, the eigenvalues of the saddle point to which the orbit is homoclinic become complex, giving a three-dimensional homoclinic orbit. For certain ratios of the eigenvalues Glendinning & Sparrow (1984) have shown that complicated bifurcation sequences including period-doubling cascades to chaos can be found near homoclinicity. Parts of these sequences were observed in Healey (1991), both in the model and in experiments.

The scenario outlined above could potentially arise whenever a Takens–Bogdanov point is found in a system with a phase space that is at least three-dimensional. At a Takens–Bogdanov point, there are two zero eigenvalues and this corresponds to $l_0 = l_1 = 0$. Applying this condition to (5.30)–(5.31) leads to

$$\cos\Phi = \left(\frac{\gamma}{2}\right)^{1/2}\left\{1 - \left(1 + \frac{1-2\gamma}{2\gamma^2}\right)^{1/2}\right\} \tag{5.33}$$

with $\delta$ then given by (5.27). Equation (5.33) only has real solutions when for $\gamma > 1/8$, otherwise the right-hand side has magnitude greater than one. The behaviour of (5.27) and (5.33) can be understood by considering a couple of limiting cases. First, let $\gamma = (1+\epsilon)/8$ where $\epsilon \ll 1$. Then it follows that

$$\Phi = \pi - 3\left(\frac{\epsilon}{5}\right)^{1/2} + O(\epsilon^{3/2}), \tag{5.34}$$

$$\delta = -\frac{3}{4}\left(\frac{5}{\epsilon}\right)^{1/2} + O(\epsilon^{1/2}). \tag{5.35}$$

In the limit $\gamma \gg 1$,

$$\Phi = \frac{\pi}{2} - \frac{1}{2(2\gamma)^{1/2}} + O(\gamma^{-3/2}), \tag{5.36}$$

$$\delta = -3\left(\frac{\gamma}{2}\right)^{1/2} + O(\gamma^{-1/2}). \tag{5.37}$$

$\Phi$ has a single minimum at $\gamma = (1+\sqrt{3})/2$ for which $\Phi \approx 1.3475$ and $\delta \approx -2.5425$. $\delta$ has a single maximum at $\gamma = 1/2$ for which $\Phi = \pi/2$ and $\delta = -2$.

A combination of numerical integrations of (5.14)–(5.16) and the analytic results obtained above have been used to elucidate the possible behaviour that can be exhibited by the resonant mode amplitude equations. The results of this study are included in Appendix B for completeness. Figures 19 and 20 give some indication of the complexity of the nonlinear dynamics that can be found in the resonant amplitude equations near the Takens–Bogdanov point.

However, in a boundary layer experiment there is no guarantee that all of this behaviour can be observed (even if a regime corresponding to suitable model parameters

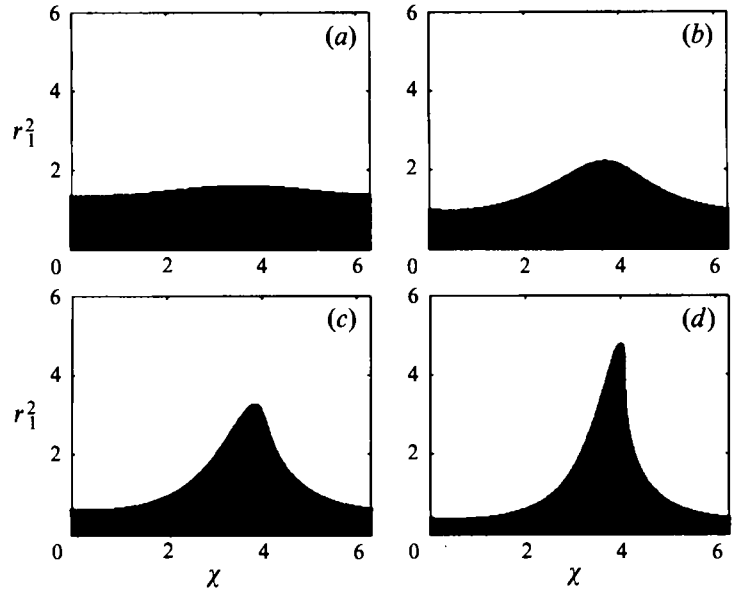


FIGURE 8. Basin of attraction for the stable fixed point at $\gamma = 0.05$, $\Phi = 2.6$ and $\delta = -4$. Black points correspond to sets of initial conditions that converge onto the fixed point, and white points are initial conditions that ultimately diverge to infinity. (*a*) $r_2 = 0.1$, (*b*) $r_2 = 0.5$, (*c*) $r_2 = 1.0$ and (*d*) $r_2 = 1.5$.

can be found), because of the slow boundary layer growth. A disturbance propagating downstream may satisfy the resonance conditions at a particular downstream location but will then be detuned away from this position. This might be modelled heuristically by allowing $\delta$ to be a slowly varying function during the integration of (5.14)–(5.16). Therefore many of the finer details described above may only exist transiently in an experiment (although they may be present in exactly parallel flows like the asymptotic suction profile or plane Poiseuille flow if this resonance occurs there too). Perhaps the most robust feature of (5.14)–(5.16) is that there can be bounded or unbounded solutions depending on the amount of detuning. In the unbounded case, a singularity occurs after finite time. The assumptions of weak growth necessary in the derivation of the amplitude equations must break down before this happens, but the enhanced destabilization of the solution by the leading-order nonlinear terms may be significant in promoting transition.

Even when a stable fixed point exists, the solution may not converge onto it unless suitable initial conditions are chosen. Figure 8 shows the basin of attraction of the stable fixed point at $\gamma = 0.05$ and $\Phi = 2.6$, which are the values at $R = 2000$ for unmodulated waves, and $\delta = -4$. Figure 8(*a*) shows the basin of attraction for initial conditions with $r_2 = 0.1$, $0 < \chi < 2\pi$ and $0 < r_1^2 < 6$. For $r_1^2 = 1$, say, then for all initial phases between the two modes, the solution converges onto the fixed point, while for $r_1^2 = 3$ all initial phases diverge. When $r_1^2 \approx 1.5$ the solution converges or diverges depending on the initial relative phase of the two modes. The phase dependence is relatively weak for $r_2 = 0.1$, but becomes much more pronounced as $r_2$ increases. In (*d*), where $r_2 = 1.5$, the amplitude of $r_1^2$ needed to cause divergence varies by a factor of order 20 with the initial phase relationship. This phase dependence will be tested for in the experiment.

## 6. Experimental investigation

Experiments have been carried out in the low-turbulence wind tunnel in the Engineering Department at Cambridge University. The experimental arrangement is essentially the same as that described in Healey (1993). A flat plate was mounted at zero incidence to an oncoming flow of air and a two-flap arrangement was used at the downstream end of the plate to obtain a zero pressure gradient over the working part of the plate. The turbulence level in the free stream (in the range 4–4000Hz) was of order 0.01% of the mean velocity of 18 m $s^{-1}$. A small loudspeaker is embedded 200 mm from the leading edge and communicates with the boundary layer via a small hole giving a point source for the disturbances. The loudspeaker can be driven by computer-generated signals via a digital to analogue (D/A) converter, and a hot-wire positioned downstream of the hole is sampled at a frequency that is phase-locked with the D/A. The same disturbance was introduced up to 200 times and the hot wire data averaged to reduce the effect of incoherent background disturbances.

When an unmodulated sinusoidal disturbance is introduced into the boundary layer it has a strong tendency to become modulated as it evolves downstream. It seems that very small amounts of irregular background noise can grow in the presence of a sinusoidal excitation and strongly modulate the signal. Figure 1 of Healey (1993) shows an example of this phenomenon, and for a more detailed discussion see Gaster (1990) where these ideas were first developed. Therefore, it is sensible to consider modulated waves from the outset, since completely unmodulated waves cannot be realized in an experiment, and especially since natural transition is dominated by irregular disturbances. Signals of the form shown in figure 4(*a*) were used so that the relative importance of sections with growing, constant and decaying amplitude could be studied simultaneously.

Figure 9 shows the effect of increasing the strength of the modulation at a particular frequency. When the damping rates are small, as in (*a*), the modulation has little effect, but as they increase, (*b*) and (*c*) start to show some increased growth near the onset of the damping part of the signal and in (*d*) a strong spike has appeared during the damping section. The amplitude of the response for the unmodulated section is several percent of the local mean flow speed, but the spike is about a quarter of the local mean flow. The results in §4 indicated that the strength of the nonlinear coefficients will be greatly enhanced if $-\omega_i/\omega_r \sim 0.1$, and the experimental results in figure 9 confirm that with sufficiently strong temporal damping in the input, there is a dramatic nonlinear breakdown.

Furthermore, the analysis in §5 indicates that the solution may either converge to a bounded solution or diverge to infinity depending on the initial phase relationship between the two resonant modes. The excitation frequency used in figure 9 is close to the unstable lower resonant frequency shown in figure 2 at almost the same $R$. The stable higher resonant frequency will be excited to some extent by the discontinuities in the first derivative of the envelope function at points where the signal switches from an unmodulated section to a modulated section. The relative phase $\chi$ between the two modes can be adjusted by changing the phase of the oscillating part relative to the modulating envelope.

Figure 10 shows two driving signals identical in every respect, except that the phase between the envelope and the oscillating part of one has been shifted by $\pi$ relative to the other. It can be seen that this simple phase shift completely changes the nonlinear behaviour of the disturbance, and suppresses the breakdown. It is possible that the large spike observed in figure 10(*a*) corresponds to the finite time singularity that can

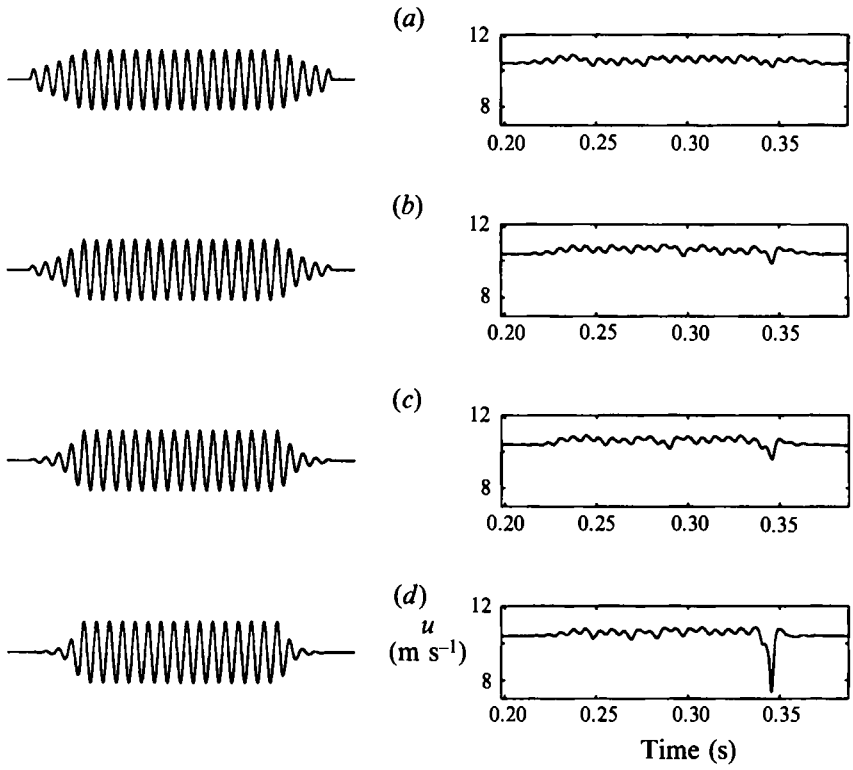


FIGURE 9. The left-hand column is a set of driving signals that have been sent to the loudspeaker, the right-hand column are the (averaged) hot-wire measurements corresponding to these inputs. The hot wire was one displacement thickness from the wall and directly downstream from the loudspeaker hole at a position where $R = 1980$. The signal has frequency $\omega_r = 0.0805$ in each case, and the following damping rates were used: (*a*) $\omega_i = 0.037$, (*b*) $\omega_i = 0.065$, (*c*) $\omega_i = 0.102$ and (*d*) $\omega_i = 0.153$.

occur in the amplitude equations and that the absence of the spike in figure 10(*b*), where the phase relationship has been changed, corresponds to the equilibrated solutions of the amplitude equations that can exist at the same parameter values and that can be reached with the appropriate initial phase relationship. Although it is difficult to make precise quantitative comparisons between the amplitude equations and the experiment, there appears to be a strong qualitative correspondence.

Figure 11 is analgous to figure 8; it shows how the strength of the breakdown observed in the experiment varies with the relative initial phase of the two modes and the amplitude of the signal. There is the same qualitative behaviour as seen in figure 8. For a small enough initial amplitude the response is small and for large enough initial amplitudes there are spikes in the hot-wire signals. However, for a range of intermediate amplitudes there is a strong dependence on the initial phase between the two modes and figure 10 shows a relatively extreme example.

The structure of the spike has also been studied in the $y$-direction. Figure 12 shows a series of hot-wire records taken from different heights in the boundary layer. The small irregular oscillations during the flat part of the input disturbance are highly reproducible through the boundary layer. Near the wall the spike has a stronger upward part, while higher up it has a stronger downward part. The spike is tilted forwards slightly: the spike observed near the edge of the boundary layer is detected at an earlier time than the spike observed near the wall. This inclination of the spike

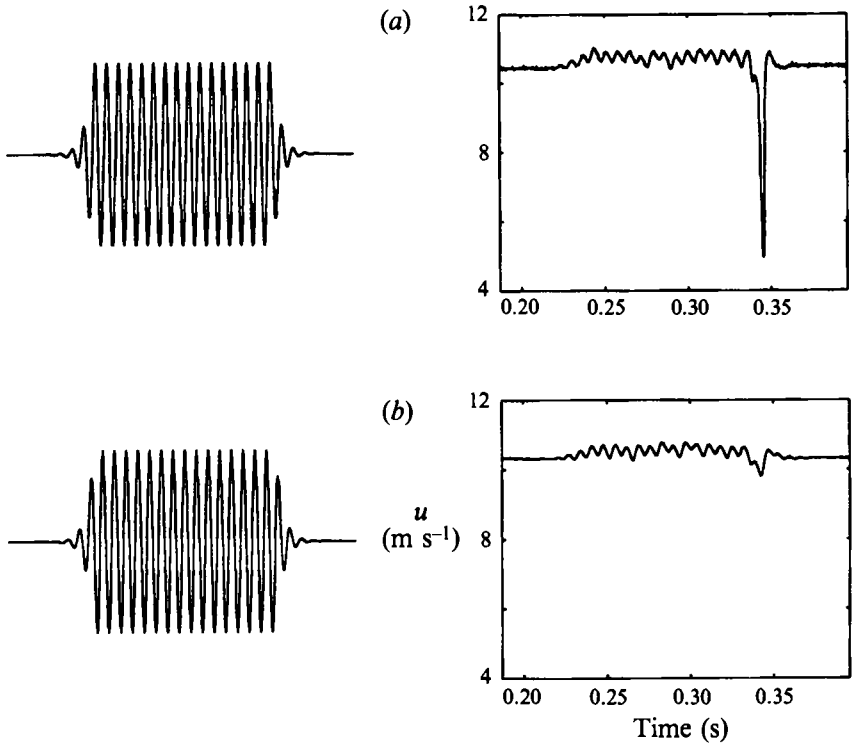


FIGURE 10. Strongly modulated waves near the resonant frequency with the same amplitude for the driving signal as in figure 9. The input signal in (*b*) is $-1$ times the input signal in (*a*). In both cases, $\omega_i = 0.21$.

through the boundary layer results in the instantaneous profiles becoming strongly inflectional as the spike passes by, see figure 13. An inflectional shear layer has formed in (*c*) and this moves downwards in (*d*) and (*e*). Inflectional profiles are inviscidly unstable and have much stronger growth rates than the Blasius profile. At later times, after the spike has passed by, the profiles become fuller than the Blasius profile and these may be less unstable than Blasius profiles (or even stable).

The disturbances have a more complicated structure in the spanwise direction. The disturbances are introduced via a point source and so oblique waves will also be present. Resonant triad-interactions are likely to occur and these will contribute to the nonlinear breakdown observed in the experiment (but excluded from the analysis). Figure 14 shows how the disturbance varies across the span of the flow. There is significant spanwise modulation of the disturbance during the constant-amplitude section showing that oblique waves play an important role in the evolution. However, the most striking feature is the spiky beakdown that occurs during the temporally decaying part of the disturbance, i.e. at the trailing edge. That the resulting breakdown is strongly three-dimensional is not surprising, the important result is that it is confined to the temporally damped section of the disturbance where the analysis of §4 showed that the nonlinear coefficients are greatly strengthened. Figure 15 shows a similar set of data but with greater resolution in the spanwise direction. This shows that the spikes are more three-dimensional than the constant-amplitude section of the input disturbance. It seems that the two-dimensional resonance described in this paper

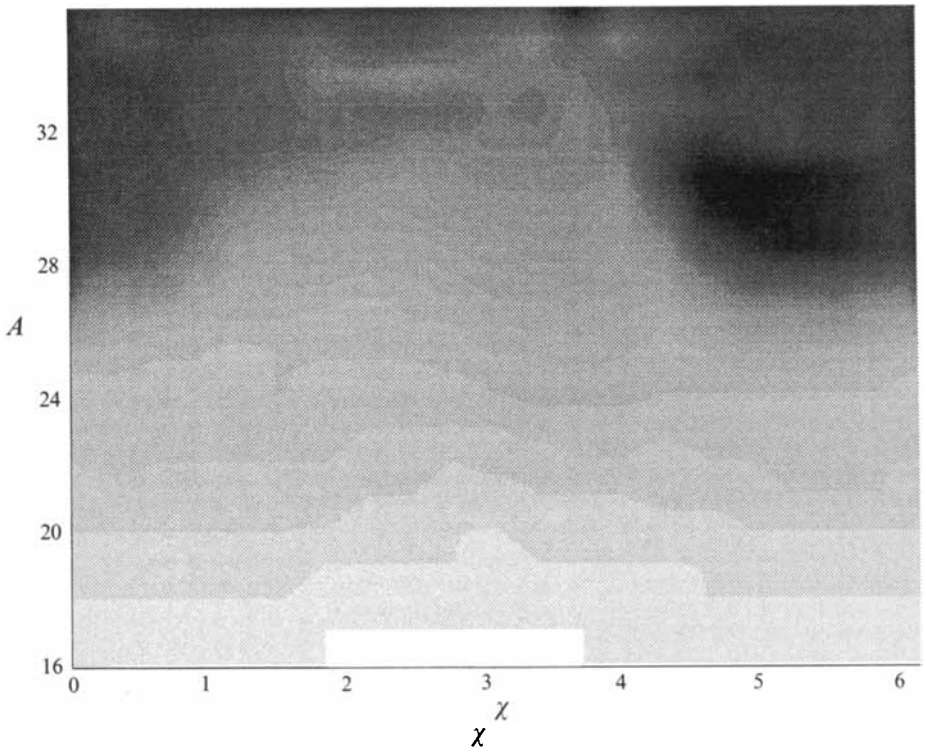


FIGURE 11. $A$ is the amplitude of the modulated input disturbance in arbitrary units and $\chi$ is the initial relative phase between the two modes (up to an arbitrary constant phase shift). The r.m.s. of the measured signal at the same position used in figures 9 and 10 is given by the greyscale: the darker the shade, the stronger the spike and the lighter shades give the smaller magnitudes of the response.

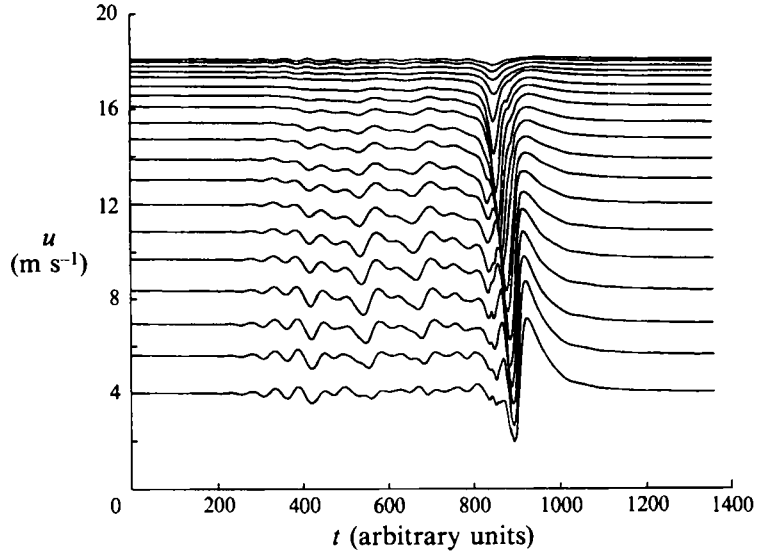


FIGURE 12. The structure of the disturbance in the $y$-direction. The vertical axis is the horizontal velocity component in m $s^{-1}$ for a set of regularly spaced heights away from the wall.

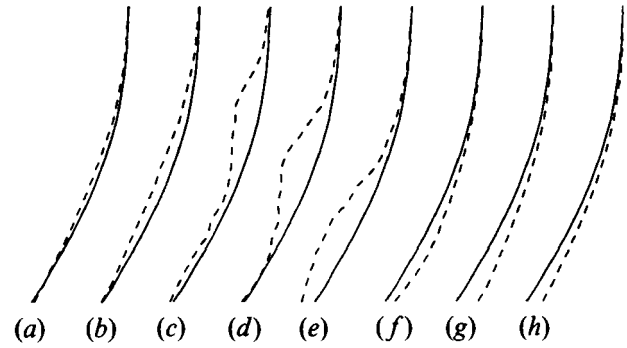


FIGURE 13. A series of instantaneous velocity profiles at times (in the same units as figure 12) of (*a*) 810, (*b*) 830, (*c*) 850, (*d*) 870, (*e*) 890, (*f*) 910, (*g*) 930 and (*h*) 950. In each plot the solid line is a measured mean profile with no disturbance and the dashed line is the instantaneous profile.

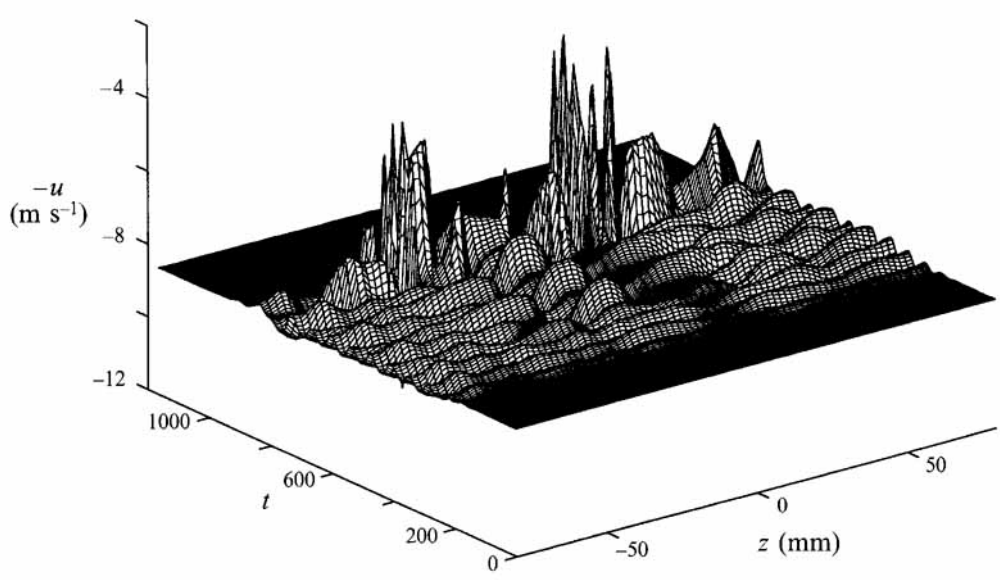


FIGURE 14. A set of hot-wire signals recorded at $R = 1980$, one displacement thickness from the wall and at 2 mm intervals in the range $-80 < z < 80$ mm, where $z = 0$ is directly downstream from the source. The time is measured in the same units as figure 12, and $-u$ has been plotted because at this height the spikes are mainly downward and would be obscured in a plot of $+u$.

causes an initial growth in the disturbance near the decaying part of the input and this stimulates a vigorous three-dimensional nonlinear interaction.

A further test can be applied to the apparent relationship between the experimental results and the theory described in §§2–5. The phase dependent breakdown observed in the experiment should disappear when the frequency of the carrier wave is sufficiently detuned from the resonance condition. A good indicator of resonant behaviour is the phase-dependence shown in figures 10 and 11, but account must also be taken of the spanwise variations. The following measure of resonant behaviour has been used. Take a spanwise traverse across the plate, e.g. figure 14, and take the total standard deviation, $\sigma_0$, of the measured disturbance from the mean undisturbed flow. Then repeat the traverse but with the input disturbance phase shifted by $\pi$ relative to the modulating envelope (in practice, multiply the input by minus one) and calculate the

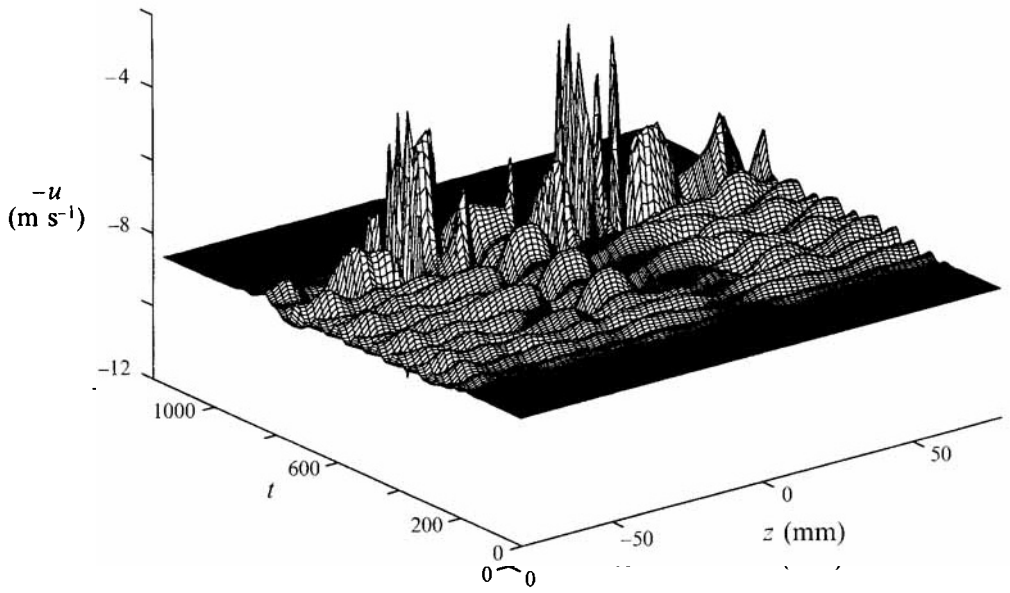


FIGURE 15. Same as figure 14 but with records taken at 0.625 mm intervals in the range $0 < z < 50$ mm.

new standard deviation, $\sigma_\pi$. Let $r_\pi = \sigma_0/\sigma_\pi$; if $r_\pi \approx 1$ then the disturbance evolution is independent of phase and the dynamics are either linear or a nonresonant nonlinear interaction. On the other hand, if $r_\pi \neq 1$ then phase-dependent resonant nonlinear behaviour is being observed. The ratio $r_\pi$ is calculated for a range of amplitudes and frequencies.

Figure 16 shows the variation of $r_\pi$ with amplitude and frequency at three different values of $R$. There is a well-defined resonant frequency in each case. The strength of the resonance decreases with decreasing $R$ and it can be seen from figure 7 that there is local maximum in the strength of the nonlinear coefficient for modulated waves near $R = 2000$. However, more experimental results need to be taken before it can be determined whether or not there is a true correlation between the strength of the resonance observed in the experiment and the strength of the nonlinear coefficients in the model. A comparison between the experimentally determined resonant frequencies and the predicted resonant frequencies is shown in figure 17. Both the OS calculations and triple-deck calculations are in excellent agreement with the experiment.

## 7. Conclusions

A new resonance has been found for two-dimensional waves in the Blasius boundary layer where the frequency and wavenumber of one wave are exactly twice those of the other wave. The lower-frequency member of the pair lies near the most unstable frequency for a given Reynolds number and the higher-frequency wave is on one of the higher-order damped branches of the dispersion relationship. Although the resonance was discovered using OS theory, it can also be found on the lower-branch asymptotic theory and so has a triple-deck structure. At large enough $R$ the resonant modes are $\omega = 2.85R^{-1/2}$, $\alpha = (1.14 - 0.149\mathrm{i})R^{-1/4}$ and $\omega = 5.70R^{-1/2}$, $\alpha = (2.28 + 0.865\mathrm{i})R^{-1/4}$.

Although the resonance has not been found for nearly neutral waves, a weakly nonlinear approach has been taken and a set of nonlinear resonant amplitude equations have been derived. Only the leading-order nonlinear terms have been calculated

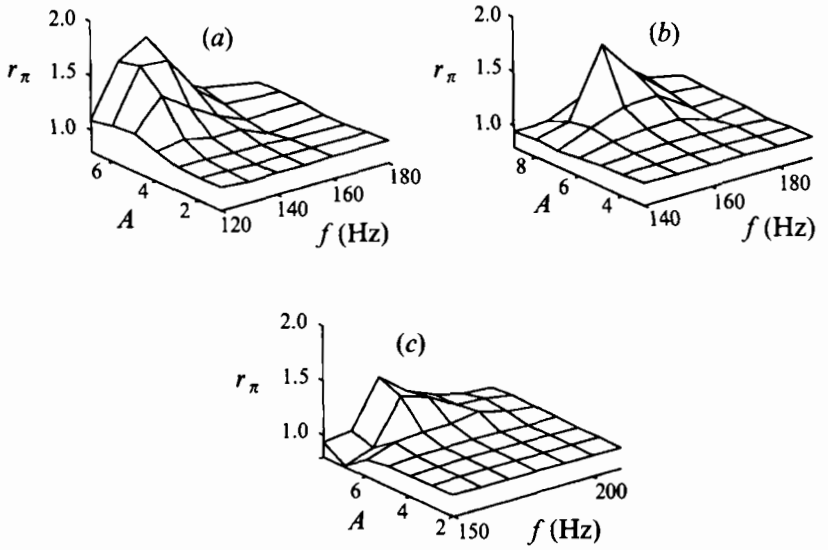


FIGURE 16. Resonant response $r_\pi$ (defined in text) as a function of the amplitude $A$ (in arbitrary units) of the disturbance and the frequency of the disturbance at (*a*) $R = 1980$, (*b*) $R = 1840$ and (*c*) $R = 1690$.

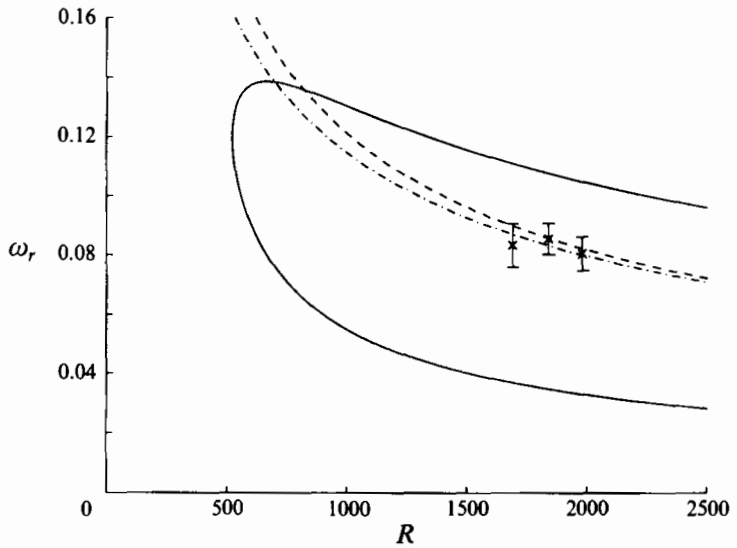


FIGURE 17. Solid line is the OS neutral curve, dashed line is the lower resonant frequency calculated using OS theory and the dot-dashed line is the resonant frequency calculated using the triple-deck dispersion relationship in Hultgren (1987). The crosses are the experimental resonant frequencies taken from the maxima in figure 16 and the error bars indicate the width of the resonant peaks in figure 16.

and the resulting truncated equations cannot be justified rigorously because of the finite growth rates. In addition, the effects of boundary layer growth have been neglected. Nonetheless, they capture certain important features of the early stages of the nonlinear behaviour and give some clues about the onset of transition.

Amplitude modulation of the waves has been modelled by allowing the frequency used in the spatial analysis to become complex. A wave whose amplitude is changing exponentially in time over enough cycles will evolve like a complex frequency for a finite period of time. The nonlinear coefficients in the amplitude equation only depend implicity on $\omega$ and so, since the dispersion relationship is analytic nearly everywhere, adding a small complex part to the frequency would not be expected to have any significant effect on the nonlinear coefficients. However, for $\omega_i \approx -0.1\omega_r$, one of the resonant modes passes close to a branch point in the dispersion relation and here substantial increases in the magnitude of the nonlinear coefficients can occur. This suggests that if a disturbance is introduced with a sufficiently strong decaying section then the decaying part may provoke a much stronger nonlinear interaction than any unmodulated sections or growing sections of the disturbance. The results of wind tunnel experiments have been presented that show that for a disturbance with a growing section, an unmodulated section and a decaying section, it is the decaying section that shows the first and strongest nonlinear behaviour.

Analytic and numerical solutions of the amplitude equations have been obtained including steady solutions, Hopf bifurcations to periodic solutions, period-doubling cascades to chaos and homoclinic orbits. A feature of these equations (and 2:1 resonant equations in general) is that the evolution of the equations can depend on the initial phase relationship between the two resonant modes. In particular, two modes with fixed initial amplitude may either diverge to infinity or converge to a steady solution depending on their initial phase relationship. Wind tunnel experiments have demonstrated that whether breakdown occurs or not does depend on the initial relative phase in the same qualitative way as the model. This phase dependence is also a feature of Craik resonant triads, but resonant triads can be found for any frequency of two-dimensional wave, whereas the resonance described in this paper exists for only one frequency at any given Reynolds number. Experiments have been carried out to find out at what frequencies this resonant behaviour can be observed. The experiments show that the resonance is confined to a narrow frequency band and this frequency agrees very well with the resonant frequency predicted by the theory.

Thus the three predictions made by the theory, namely (i) a certain resonant frequency exists, (ii) the nonlinear behaviour depends on the relative phase of the modes and (iii) the nonlinear behaviour can be enhanced by decaying sections in the input disturbance, have all been confirmed by experimental measurements in a wind tunnel. This agreement may be taken as a retrospective justification for the assumptions made in the derivation of the amplitude equations.

The discovery of a particular dangerous frequency with a dangerous type of modulation, that promotes the nonlinear breakdown of a disturbance, has important implications for transition prediction on aerofoils.

This work was supported by the Engineering and Physical Sciences Research Council of the UK under its Applied Nonlinear Mathematics Initiative.

## Appendix A

The derivation of the amplitude equations is presented in this Appendix. The disturbance equations (3.5)–(3.7) are substituted into the continuity and Navier–

Stokes equations:

$$\left(\frac{\partial}{\partial x}+\epsilon\frac{\partial}{\partial X}\right)u+\frac{\partial v}{\partial y}=0, \tag{A 1}$$

$$\frac{\partial u}{\partial t}+u\left(\frac{\partial}{\partial x}+\epsilon\frac{\partial}{\partial X}\right)u+v\frac{\partial u}{\partial y}=-\left(\frac{\partial}{\partial x}+\epsilon\frac{\partial}{\partial X}\right)p + \frac{1}{R}\left(\left[\frac{\partial^2}{\partial x^2}+2\epsilon\frac{\partial^2}{\partial x\partial X}\right]u+\frac{\partial^2 u}{\partial y^2}\right), \tag{A 2}$$

$$\frac{\partial v}{\partial t}+u\left(\frac{\partial}{\partial x}+\epsilon\frac{\partial}{\partial X}\right)v+v\frac{\partial v}{\partial y}=-\frac{\partial p}{\partial y}+\frac{1}{R}\left(\left[\frac{\partial^2}{\partial x^2}+2\epsilon\frac{\partial^2}{\partial x\partial X}\right]v+\frac{\partial^2 v}{\partial y^2}\right), \tag{A 3}$$

where (3.8) has been used for the spatial derivatives. Where $\alpha_r$ appears in $E$ it is replaced by $\alpha^{(1)}+\mathrm{i}\epsilon$ and where $2\alpha_r$ appears in $E^2$ it is replaced by $\alpha^{(2)}-\Delta\epsilon-\mathrm{i}\epsilon/\gamma$ using (3.1) and (3.2). Terms of $O(\epsilon)$ are then gathered together as are terms of $O(\epsilon^2)$. The resulting sets of equations are in $u$, $v$ and $p$; further manipulation eliminates $u$ and $p$ to give equations in $v$ only.

At $O(\epsilon)$ the coefficient of $E$ is

$$\mathrm{L}_1(v_1)=0 \tag{A 4}$$

where $\mathrm{L}_1$ is the OS operator defined as the left-hand-side of (2.3) with $\alpha=\alpha^{(1)}$ and $\omega$ is the resonant frequency. The coefficient of $E^2$ is

$$\mathrm{L}_2(v_2)=0 \tag{A 5}$$

where $\mathrm{L}_2$ is the OS operator with wavenumber $\alpha^{(2)}$ and $\omega$ is twice the resonant frequency. At this order in $\epsilon$, the modes are uncoupled and (A 4) and (A 5) simply define the linear eigenfunctions of the resonant modes.

At $O(\epsilon^2)$ the coefficient of $E$ is

$$\mathrm{L}_1(v_{21})=(A_1-\dot{A}_1)f_1+A_1^*A_2g_1 \tag{A 6}$$

where the dot represents differentiation with respect to $X$, the star denotes the complex conjugate and

$$f_1=\frac{\omega}{\alpha_1}\left(v_1''+\alpha_1^2v_1\right)-2\alpha_1^2Uv_1-\frac{\mathrm{i}}{\alpha_1\mathrm{R}}\left(v_1''''+2\alpha_1^2v_1''-3\alpha_1^4v_1\right), \tag{A 7}$$

$$g_1=\frac{\alpha_1^2}{\alpha_2}(\alpha_1+\alpha_2)v_1^*v_2'+\frac{\alpha_1^2}{\alpha_1^*}\left(\alpha_1^*+\alpha_2\right)v_1'^*v_2 + \frac{\left(\alpha_1^2-|\alpha_1|^2-\alpha_1\alpha_2\right)}{\alpha_1^*\alpha_2}v_1'^*v_2''+\frac{\alpha_1^2}{\alpha_1^*\alpha_2}v_1''^*v_2'-\frac{\alpha_1}{\alpha_2}v_1^*v_2'''+\frac{\alpha_1}{\alpha_1^*}v_1''''^*v_2, \tag{A 8}$$

where for notational convenience $\alpha_1=\alpha^{(1)}$ and $\alpha_2=\alpha^{(2)}$. The coefficient of $E^2$ is

$$\mathrm{L}_2(v_{22})=-\left([\gamma^{-1}-\mathrm{i}\Delta]A_2+\dot{A}_2\right)f_2+A_1^2g_2 \tag{A 9}$$

where

$$f_2=\frac{2\omega}{\alpha_2}\left(v_2''+\alpha_2^2v_2\right)-2\alpha_2^2Uv_2-\frac{\mathrm{i}}{\alpha_2\mathrm{R}}\left(v_2''''+2\alpha_2^2v_2''-3\alpha_2^4v_2\right), \tag{A 10}$$

$$g_2=\frac{\alpha_2}{\alpha_1}(v_1'v_1''-v_1v_1'''). \tag{A 11}$$

The condition that the inhomogeneous equation (A 6) should have nontrivial solutions is that its right-hand side should be orthogonal to the solutions of the adjoint homogeneous problem with homogeneous boundary conditions, see Ince (1956, §9.34). The adjoint of (2.3) is

$$(\alpha U - \omega)(\psi'' - \alpha^2\psi) + 2\alpha U'\psi' + \frac{\mathrm{i}}{\mathrm{R}}(\psi'''' - 2\alpha^2\psi'' + \alpha^4\psi) = 0, \tag{A 12}$$

where $\psi$ is the solution of the adjoint problem satisfying the boundary conditions $\psi = \psi' = 0$ at $y = 0$ and as $y \to \infty$. The eigenvalues of (A 12) are the same as the eigenvalues of (2.3). Thus the solvability condition for (A 6) is

$$\int_0^\infty \left([A_1 - \dot{A}_1]f_1 + A_1^* A_2 g_1\right)\psi_1 \mathrm{d}y = 0 \tag{A 13}$$

where $\psi_1$ is the eigenfunction of (A 12) when $\alpha = \alpha_1$. A similar requirement applies to (A 9) and leads to the solvability condition

$$\int_0^\infty \left(-\left[(\gamma^{-1} - \mathrm{i}\Delta)A_2 + \dot{A}_2\right] f_2 + A_1^2 g_2\right)\psi_2 \mathrm{d}y = 0 \tag{A 14}$$

where $\psi_2$ is the eigenfunction of (A 12) when $\alpha = \alpha_2$. Re-writing (A 13) and (A 14) leads to the complex amplitude equations (3.9)–(3.10) where

$$a = \int_0^\infty g_1\psi_1 \mathrm{d}y \Big/ \int_0^\infty f_1\psi_1 \mathrm{d}y, \tag{A 15}$$

$$b = \int_0^\infty g_2\psi_2 \mathrm{d}y \Big/ \int_0^\infty f_2\psi_2 \mathrm{d}y. \tag{A 16}$$

## Appendix B

This Appendix contains the results of numerical integrations of the resonant-mode equations (5.14)–(5.16) combined with the analytical results obtained in §5. It is convenient to study $(\Phi, \delta)$ parameter planes for different constant values of $\gamma$.

Figure 18 shows the $(\Phi, \delta)$ parameter plane for $\gamma = 0.3$. The region in between the two lines $s$ in ($a$) has two fixed points and outside this region there are no fixed points and all nontrivial solutions are unbounded. For most of the region between the saddle-node bifurcations there is one stable fixed point and one unstable fixed point. However, in moving across the line $h$ it is found that $l_0 = l_1 l_2$ and $l_1 > 0$ and so the stable fixed point loses stability via a Hopf bifurcation. Numerical solutions near these parameter values confirm that a stable limit cycle exists immediately to the right of $h$. As $\Phi$ is increased with $\delta = -3.5$, say, the amplitude of the limit cycle grows until it approaches the unstable fixed point and becomes homoclinic near the dashed line. A further increase in $\Phi$ leads to unbounded solutions. The Hopf bifurcation and locus of homoclinic orbits originate from the Takens–Bogdanov point marked by the '+'. At more negative values of $\delta$, the limit cycle undergoes a period-doubling bifuraction at $p_2$ before becoming homoclinic. In fact, within the very narrow region of parameter space between the dashed line and $p_2$, a whole period-doubling cascade to chaotic solutions can be found. This narrow region appears to persist for large negative $\delta$ (and this might be an interesting limit to study), but must necessarily terminate before reaching the Takens–Bogdanov point where the dynamics are two-dimensional and so cannot support chaos.

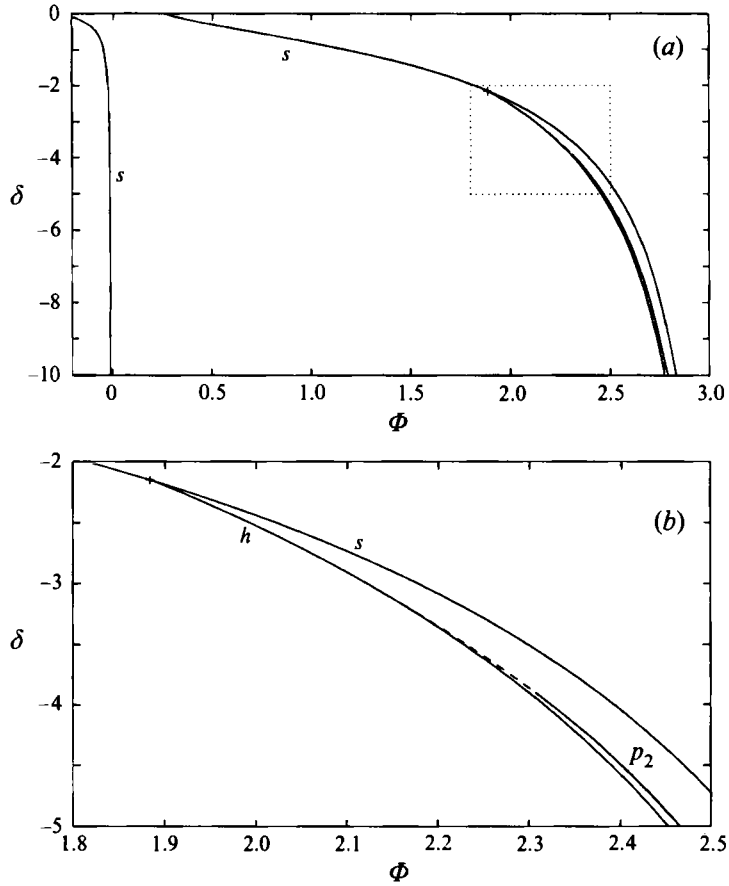


FIGURE 18. Parameter-space maps for $\gamma = 0.3$. Lines marked $s$ correspond to points where a saddle-node bifurcation occurs and were calculated using (5.27). (*b*) An enlargement of the region enclosed within the dotted box shown in (*a*). The '+' sign indicates the location of the Takens–Bogdanov point calculated using (5.33) and the line marked $h$ is where a Hopf bifurcation was detected. The dashed line shows where the periodic orbit created at $h$ is destroyed by a homoclinic orbit. The solid line $p_2$ shows where the periodic orbit undergoes a period-doubling bifurcation before becoming homoclinic.

As $\gamma$ is reduced the lines $s$ are qualitatively unchanged, but the Takens–Bogdanov point moves to lower $\delta$, period-doublings are no longer observed at moderate $\delta$ and the gap between $h$ and $s$ gets much thinner. When $\gamma \to 1/8$ from above the Takens–Bogdanov point has $\delta \to -\infty$ and $\Phi \to \pi$ from (5.34) and (5.35). For $\gamma < 1/8$ the stable fixed point created in the saddle-node bifurcations is always stable: no secondary bifurcations have been found.

For larger values of $\gamma$ the line $h$ moves left across the diagram and the region where chaotic solutions can be found gets larger. Figure 19 shows the $(\Phi, \delta)$-plane at $\gamma = 0.7$. The chaotic regions are now much broader than before and several further period-doubling bifurcations can be resolved. In (*b*) two lines of period-8 bifurcations cross over, but each line corresponds to bifurcations of two co-existing period-4 solutions so there is no degeneracy. These sequences of period-doubling bifurcations, reverse period-doubling bifurcations and multiple co-existing periodic states near a homoclinic orbit are characteristic of the Silnikov behaviour described

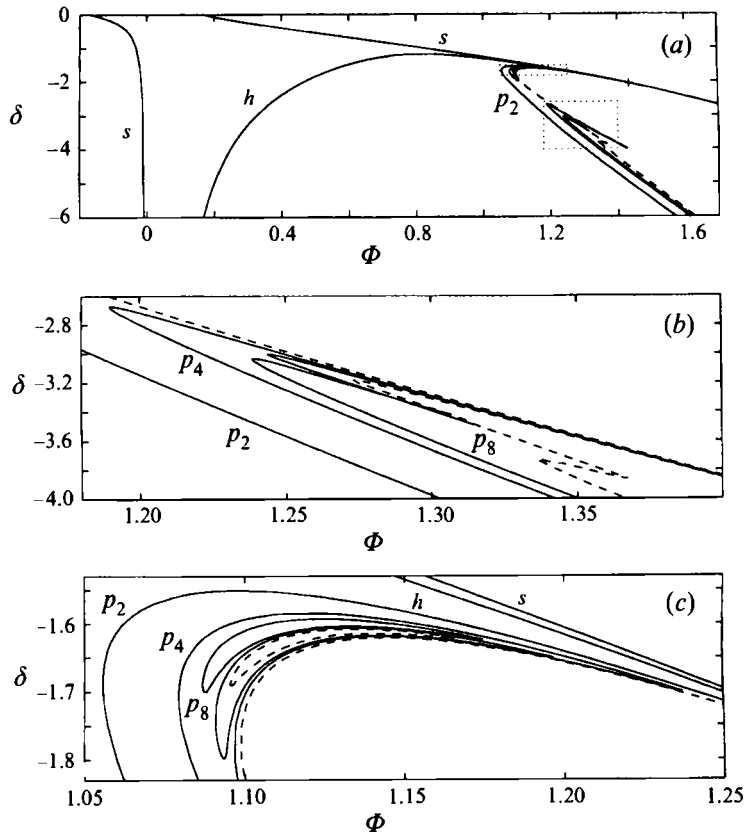


FIGURE 19. Parameter plane at $\gamma = 0.7$: (*b*) and (*c*) are enlargements of the dotted boxes shown in (*a*). The meanings of *s*, *h*, $p_2$, the dashed lines and the '+' are the same as in figure 18. The solid lines marked $p_4$ and $p_8$ are further period-doubling bifurcations giving periods of four and eight times that of the original limit cycle. Plots (*b*) and (*c*) both show sequences of period-doubling bifurcations to chaos and also reverse period-doubling bifurcations back down to lower-period limit cycles.

in Glendinning & Sparrow (1984) and found in experiments by Healey *et al.* (1991). In (*b*) the dashed line, which separates bounded from unbounded solutions, has a complicated shape and in (*c*) it has a closed loop inside the region that otherwise has bounded solutions.

Figure 20 shows a bifurcation diagram obtained by taking $\gamma = 0.7$ and $\delta = -3.3$. As $\Phi$ is increased, the limit cycle that originated from the Hopf bifurcation period-doubles to a period-2 orbit at $\Phi = 1.2181$, to a period-4 orbit at $\Phi = 1.2561$ and to a period-8 orbit at $\Phi = 1.2650$. There is a chaotic band (with periodic windows) until $\Phi = 1.2865$ where there is a reverse period-doubling bifurcation that turns a period-8 orbit into a period-4 orbit. This period-4 orbit is then destroyed by a periodic saddle-node bifurcation at $\Phi = 1.2869$. A second period-4 orbit is created at a periodic saddle-node bifurcation at $\Phi = 1.2862$, and there is hysteresis between these two stable solutions as $\Phi$ is increased and decreased. This second period-4 orbit bifurcates to a period-8 orbit at $\Phi = 1.2865$ (which happens to be where the reverse period-doubling bifurcation occurs on the other solution, this explains the crossing of the $p_8$ lines in figure 19*b*). A second band of chaotic solutions then follows shortly afterwards until at $\Phi = 1.2893$ the chaotic solution diverges to infinity. By using suitable initial

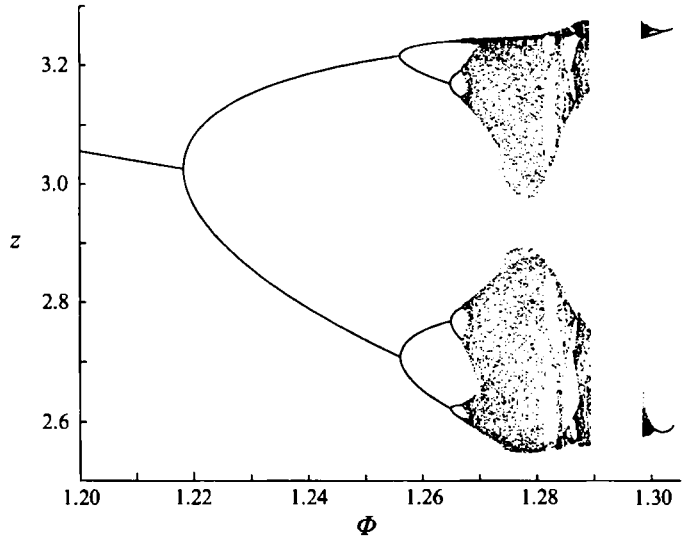


FIGURE 20. Bifurcation diagram for $\gamma = 0.7$ and $\delta = -3.3$. Equations (5.14)–(5.16) were integrated and the $z$-coordinate of the Poincaré section defined by the plane $x = -\gamma$ has been plotted as a function of $\Phi$.

conditions a third chaotic band can be found starting at $\Phi = 1.2984$ and a reverse period-doubling bifurcation producing a period-4 orbit occurs at $\Phi = 1.3003$. This period-4 orbit reverse period-doubles at $\Phi = 1.3018$ and the resulting period-2 orbit is destroyed by a periodic saddle-node bifurcation at $\Phi = 1.3039$; no bounded solutions have been found for $\Phi > 1.3039$ at this value of $\delta$.

## REFERENCES

BERTOLOTTI, F. P., HERBERT, T. & SPALART, P. R. 1992 *J. Fluid Mech.* **242**, 441–474.

BODONYI, R. J. & SMITH, F. T. 1981 *Proc. R. Soc. Lond.* A **375**, 65–92.

CRAIK, A. D. D. 1971 *J. Fluid Mech.* **50**, 393–413.

CRAIK, A. D. D. 1985 *Wave Interactions and Fluid Flows.* Cambridge University Press.

DAVEY, A. 1982 In *Stability in the Mechanics of Continua* (ed. F. H. Schroeder), pp. 365–372. Springer.

FARGE, M. 1992 *Ann. Rev. Fluid Mech.* **24**, 395–457.

FFOWCS WILLIAMS, J. E. & GUO, Y. P. 1991 *J. Fluid Mech.* **224**, 507–529.

GASTER, M. 1979 In *Proc. IUTAM Symp. on Laminar–Turbulent Transition* (ed. R. Eppler & H. Fasel), pp. 14–16. Springer.

GASTER, M. 1990 *Proc. R. Soc. Lond.* A **430**, 3–24.

GLENDINNING, P. & SPARROW, C. 1984 *J. Statist. Phys.* **35**, 645–696.

GOLDSTEIN, M. E. & LEE, S. S. 1992 *J. Fluid Mech.* **245**, 523–551.

GUCKENHEIMER, J. & HOLMES, P. 1986 *Nonlinear Oscillations, Dynamical Systems and Bifurcations of Vector Fields*, 2nd edn. Springer.

HEALEY, J. J. 1993 *J. Fluid Mech.* **255**, 667–681.

HEALEY, J. J. 1994 *Phys. Rev. Lett.* **73**, 1107–1109.

HEALEY, J. J. 1995*a* *J. Fluid Mech.* **288**, 59–73.

HEALEY, J. J. 1995*b* In *Proc. IUTAM Symp. on Laminar-Turbulent Transition* (ed. R. Kobayashi), pp. 437–444. Springer.

HEALEY, J. J. 1995*c* A comparison between Orr–Sommerfeld theory and asymptotic theories for damped and growing boundary layer modes. *J. Fluid Mech.* (Submitted).

HEALEY, J. J., BROOMHEAD, D. S., CLIFFE, K. A., JONES, R. & MULLIN, T. 1991 *Physica* D **48**, 322–339.

HICKERNELL, F. J. 1984 *J. Fluid Mech.* **142**, 431–449.
HOCKING, L. M. 1975 *Q. J. Mech. Appl. Maths* **28**, 341–353.
HUGHES, D. W. & PROCTOR, M. R. E. 1990 *Physica* D **46**, 163–176.
HUGHES, D. W. & PROCTOR, M. R. E. 1992 *J. Fluid Mech.* **244**, 583–604.
HULTGREN, L. S. 1987 *Phys. Fluids* **30**, 2947–2951.
INCE, E. L. 1956 *Ordinary Differential Equations.* Dover.
KELLY, R. E. 1968 *J. Fluid Mech.* **31**, 789–799.
KLINGMANN, B. G. B., BOIKO, A. V., WESTIN, K. J. A., KOZLOV, V. V. & ALFREDSSON, P. H. 1993 *Eur. J. Mech.* B/*Fluids* **12**, 493–514.
LIN, C. C. 1955 *The Theory of Hydrodynamic Stability.* Cambridge University Press.
MANKBADI, R. R., WU, X. & LEE, S. S. 1993 *J. Fluid Mech.* **256**, 85–106.
PROCTOR, M. R. E. & JONES, C. A. 1988 *J. Fluid Mech.* **188**, 301–335.
RAETZ, G. S. 1959 A new theory of the cause of transition in fluid flows. *Norair, Rep. NOR*-59-383. California: Hawthorne.
REID, W. H. 1965 In *Basic Developments in Fluid Dynamics*, vol. I (ed. M. Holt), pp. 249–307. Academic.
SHAIKH, F. N. & GASTER, M. 1994 *J. Engng Maths* **28**, 55–71.
SMITH, F. T. 1979 *Proc. R. Soc. Lond.* A **366**, 91–109.
SMITH, F. T. & BURGGRAF, O. R. 1985 *Proc. R. Soc. Lond.* A **399**, 25–55.
SMITH, F. T. & STEWART, P. A. 1987 *J. Fluid Mech.* **179**, 227–252.
STEWARTSON, K. & STUART, J. T. 1971 *J. Fluid Mech.* **48**, 529–545.